Michigan Technological University
Digital Commons @ Michigan Tech

Dissertations, Master's Theses and Master's Reports - Open

Dissertations, Master's Theses and Master's Reports

2015

AN ENERGY BASED MINIMUM-TIME OPTIMAL CONTROL OF DC-DC CONVERTERS

Amir Zandnia
Michigan Technological University

Follow this and additional works at: https://digitalcommons.mtu.edu/etds

 Part of the Electrical and Computer Engineering Commons

Copyright 2015 Amir Zandnia

Recommended Citation

Zandnia, Amir, "AN ENERGY BASED MINIMUM-TIME OPTIMAL CONTROL OF DC-DC CONVERTERS", Master's Thesis, Michigan Technological University, 2015.
https://doi.org/10.37099/mtu.dc.etds/932

Follow this and additional works at: https://digitalcommons.mtu.edu/etds

 Part of the Electrical and Computer Engineering Commons

AN ENERGY BASED MINIMUM-TIME OPTIMAL CONTROL OF DC-DC CONVERTERS

By

Amir Zandnia

A THESIS

Submitted in partial fulfillment of the requirements for the degree of

MASTER OF SCIENCE

In Electrical Engineering

MICHIGAN TECHNOLOGICAL UNIVERSITY

2015

© 2015 Amir Zandnia

This thesis has been approved in partial fulfillment of the requirements for the Degree of MASTER OF SCIENCE in Electrical Engineering.

Department of Electrical & Computer Engineering

Thesis Advisor: *Dr. Wayne W. Weaver*

Committee Member: *Dr. Gordon G. Parker*

Committee Member: *Dr. Lucia Gauchia Babe*

Department Chair: *Dr. Daniel R. Fuhrmann*

Table of Contents

Abstract

Time-optimal response is an important and sometimes necessary characteristic of dynamic systems for specific applications. Power converters are widely used in different electrical systems and their dynamic response will affect the whole system. In many electrical systems like microgrids or voltage regulators which supplies sensitive loads fast dynamic response is a must. Minimum time is the fastest converter to compensate the step output reference or load change. Boost converters as one of the wildly used power converters in the electrical systems are aimed to be controlled in optimal time in this study. Linear controllers are not able to provide the optimal response for a boost converter however they are still useful and functional for other applications like reference tracking or stabilization. To obtain the fastest possible response from boost converters, a nonlinear control approach based on the total energy of the system is studied in this research. Total energy of the system considers as the basis for developing the presented method, since it is easy and accurate to measure besides that the total energy of the system represents the actual operating condition of the boost converter. The detailed model of a boost converter is simulated in MATLAB/Simulink to achieve the time optimal response of the boost converter by applying the developed method. The simulation results confirmed the ability of the presented method to secure the time optimal response of the boost converter under four different scenarios.

Chapter 1: Introduction

Power converters have various power ranges and applications. They are almost anywhere that electric power is consumed. Low power applications are used in electronic devices, like home appliances and cellphones; medium range power converters are used in electric and hybrid vehicles; and high range power converters in microgrids, data centers and power generation sites. Another categorizing of power converters focuses on their performance and reliability. For example airplanes, spacecrafts or satellites need systems with very high reliability and dynamic performance [**1**,**2**]; that's why any movement or strategy for designing a converter with better dynamic performance is important and valuable [3**,4,**5].

Optimal dynamic response has different aspects including minimal overshoot and undershoot or minimal settling time. For different applications, it is important to minimize one of these aspects. For example, converters supplying sensitive loads need to have very small overshoot and undershoot, while in some applications, fast response is more important. Different studies were conducted to develop methods to minimize settling time and vibration of systems. Input shaping, time-optimal control and bang-bang control are the most common methods which will be discussed in the background chapter.

Optimal dynamic response is a point of interest in many different systems including flexible mechanism, servo mechanisms, robotics, power systems, power converters and many other systems. As an example of power converters, boost converters are nonlinear

dynamic system and need to be linearized before any linear controller aimed to be designed for the boost converter. In linearization, it is assumed that the converter operation range is small and the controller is working in that linear range. On the other hand, optimal response for a nonlinear system won't be achieved with linear control, and nonlinear controllers are needed to solve the optimality problem. This study is focused on optimal time control of a dc-dc boost converter to drive the system from an initial state to a final state in minimum time. As mentioned, getting the minimum time response for a boost converter needs a nonlinear controller; in Chapter 2, some nonlinear controllers are introduced and their features are discussed. A brief explanation on the reason for choosing nonlinear controllers and an example of linear controller for the boost converter is presented in Chapter 3. Chapter 4 contains method, theory and simulations for the problem and Chapter 5 comprises of conclusion and future works.

Chapter 2: Background

In this chapter, different methods for controlling a system in a manner to get minimum-time response or minimizing the system vibration during a transition are discussed. It will start by reviewing input shaping methods; afterwards, minimum-time control techniques are studied; and at the end, similar works will be reviewed and discussed.

In 1988 Singer and Seering published a paper [6] named "Preshaping Command Inputs to Reduce System Vibration." This paper is one of the most important references for input shaping because the theory basis of this method is developed and presented in this study. First, the system response to an impulse input is specified. Based on this response, a shaped input will be generated containing two impulses. The second impulse will be generated during the input or at the "end" of input to cancel all vibrations formed because of the first impulse. The logic behind this approach is that the output response for the second impulse is a mirror of the first impulse vibrations. The desired output is the combination of those two responses without vibration. Because calculating the second impulse response for the system is based on the system impulse response, having zero vibration in the output depends on having the exact values for the natural frequency and the damping ratio of the system. In hardware applications, there are always errors in calculating these properties of a system, so some techniques have to be applied to increase the robustness of the system. In this paper, Singer and Seering added additional constraints to the system and increased the input robustness for system frequency variations of around 20%. The study also describes that

by expanding this technique, the robustness would be increased for systems with up to 40% of variations in system frequency. There is always uncertainty for this method, because it is closely dependent on system modeling, so modeling errors will cause vibrations in the system output. Input shaping has various applications such as control of cranes to move without oscillation [7,8] or controlling the slewing spacecraft [9]. Input shaping is also applied to solve the trajectory following problems [10,11].

Later in 1996, Singhose, Seering and Singer present a procedure for specifying the degree of robustness and discuss some characteristics of impulse sequences [12]. They present four categories for constraint equations and amplitude of the impulses for input shaping. The first constraint is defined to obtain the impulse amplitudes having positive values for all the impulses; it prevents them to be driven to positive and negative infinity by the time optimality constraint. Another amplitude constraint forces the sum of all impulse responses to one; this constraint will force the shaped command to reach the same set point as the unshaped command. Two more constrains are also presented to improve residual vibration amplitude and robustness. Solving the set of four previous constraints will give an infinite number of solutions so another constraint is needed to make the answer singular. This final constraint minimizes the time for impulses which insures the response is time optimal. Two other solutions are also presented for shapers with specified insensitivity. One of the presented procedures is easy to formulate but must be optimized numerically because of its large number of constraints. The other procedure has fewer numbers of constraints which help to get the exact solution, but it is more difficult to formulate. Two studies on input shaping method are reviewed so far and benefits and drawbacks are also discussed. One more study on multi-input shaping

using s-plane pole placement techniques will be reviewed and then we will move to time-optimal methods.

Vibration reduction is another application of the input shaping which is presented with different approaches [13,14], Pao also published a paper [15] titled "Multi-input shaping design for vibration reduction" focused on shaping inputs for multiple input systems. Before that, most of the input shaping for multiple input systems was taking place by simply using separate shapers for each individual input. This means each input in the system is responsible for canceling out its own vibration; however in a multiple input system, inputs can be shaped in such a way to cancel or reduce output vibrations even if they are caused by other inputs. This approach gives a sequence of impulses with shorter time. Pao developed her method based on extending the zero placement technique presented by Tuttle and Seering [16] in s-plane for multiple input systems. In her method, zeros are placed at poles of each row of the system transfer matrix, formed by using the information in the inputs multiplier matrix of the system model. This gives simpler input shapers than having those zeros at all the flexible system poles. This method is simpler in formulation and has faster response in outputs; but robustness of the method should be analyzed, because there is always a tradeoff between fast response and robustness of the system. Later in 2002, Singh and Singhose published a tutorial [17] on input shaping of flexible structure which was almost the same method as previous studies but with some constraints to increase system robustness against modeling errors. This paper has gathered almost all approaches in input shaping together and compared them for different applications.

Input shaping designs are reviewed and it is mentioned that solutions for input shaping will give infinite number of solutions and the one with minimum time sequence is the answer which can be found with numerical methods. It is not guaranteed that the shortest answer is the one came out from numerical method minimization. Pao and Singhose investigated equivalence of minimum time input shaping with traditional time-optimal control [18] in several input shaping designs. They studied optimal zero-vibration (ZV) shaper, time optimal zero-vibration, zero-derivative shaper and time optimal extra-insensitive (EI) shaper methods. With their investigation, the above mentioned shapers are equivalent to traditional time-optimal control, augmented of the same system with two poles at each of the poles of the original system, and time-optimal control for a system with two poles near each of the original system poles respectively. As the authors conclude, these equivalences allows researcher to apply numerical methods for solving time-optimal control problems for input shaping. This guaranties that there is an optimal solution existing and also verifies optimality of input shaper designs. Authors also conclude that the time-optimal input shaping designs must be bang-bang and this is one of the reasons that bang-bang control is going to be investigated in this study.

By using Pontryagin's minimum principle, it can be proved that bang-bang controller with (n-1) switching is always the time-optimal solution for an (n) order system [19]**.** The main challenges for bang-bang time-optimal control are calculating the proper switching time [20] and sensitivity of this method to parameter variation [21]**;** so there are lots of studies on this topic and they suggest different methods to get the desirable result [22,23,24]. Shen and Anderson presented a method to find the switching times in

equivalence to finding a crossing point of two spiral curves under an affine mapping [25]. They modeled a second order system and formed the cost function and Hamiltonian for the problem of driving the system from an initial state to a final state. They came up with a solution with arbitrary value for input in some conditions which cannot be solved with analytic solutions because of lack of boundary conditions. To solve the problem they assumed that the control signal has its maximum value at the beginning of bang-bang control and then change to its minimum value after a certain time and remain until final time. With this assumption they reduced the problem to a second order system of equations and then interpreted the problem as finding the crossing point of the curves defined by the two sides of this equation system. With the presented method, the minimizing problem will be solved faster but using this method for higher order systems needs huge formulation. On the other hand, the affine mapping depends on the system dynamic, initial state and input bounds of the system; besides that, modeling errors would affect the solution as well.

Another study taken place by Sadegh and Driessen named “Minimum Time Trajectory Optimization and Learning” [26] adds learning algorithm to improve robustness of the system for modeling error. They used on-line measurement of the state trajectory to obtain the learning algorithm which will increase the robustness to mismatch between the model and the system. They used switching time intervals as optimization variables with this assumption that a bang-bang control solution exists to transfer the system from an initial state to a final state. Gradient optimization algorithm with freedom to add or remove switching interval is used in this paper. The final solution from this algorithm is checked to be optimal with testing against Pontryagin’s Minimum Principle. Learning

algorithm started with applying the switching control law to the actual system (which is produced from a switching interval vector calculated by the gradient optimization algorithm), and recording the final state error. Afterwards an improved switching interval is calculated and this learning interval will continue until it reaches a feasible and near optimal solution satisfying the terminal state requirement. This time-optimal solution is improved with learning algorithm to increase the robustness of the system against modeling errors, but again time optimization for switching intervals needs heavy formulation which would be very difficult for higher order systems or systems with multiple inputs.

Some papers which studied input shaping methods for reducing output vibration has been reviewed; equivalence of input shaping and time-optimal control with some examples on minimum time control is also discussed. Almost all the discussed papers and studies were focused on the theoretical part of the problem with simple practical or numerical examples in some cases. Now it is time to review some literatures on applying similar approaches on power electronic converters which is the main purpose in this study. Fuzzy logic approximation method utilized to obtain minimum-time control for a buck converter in [27], and there are also some studies tried to develop an optimum design for buck converter [28,29]. Upcoming paragraphs will be reviewing some other papers on time optimal control of a buck or a boost converter with different approaches. Benefits and drawbacks of methods will be discussed.

Rafiei, Amirahmadi and Griva, applied a game theory approach for optimizing the settling time and overshoot of a boost converter [30]. They used Strength Pareto

Evolutionary Algorithm (SPEA) to optimize the multi-objective problem. In this study, a PID controller's gains are taken as design variables to optimize the settling time and overshoot of the system. After running SPEA for a boost converter running at 15 kHz frequency with 5 volts input supply and 12 volts at the output terminal, a set of PID controllers' constants will be given as the optimal answers. Some of them has shorter settling time while some others has smaller overshoot; authors stated that one can choose any of them based on application or their own engineering view. It is known that game theory algorithm is aimed to optimize the multi-objective problems in such a way to satisfy optimality for both objectives. Most of the time, in the actual systems the optimal point for an objective is non-optimal for the others.

It is recognized that the exact time-optimal control methods might be impractical [21], as a result some studies has taken place on proximate time-optimal control [31,32]. A more practical paper published in 2007 named "Proximate Time-Optimal Digital Control for dc-dc Converters" [33] combined a PID controller and non-linear switching surface to obtain a near time-optimal control for a buck converter. Authors claimed that their approach of mixing linear PID and time-optimal controller will make it possible to have robustness, fast large signal response and precise control in steady state together. Switching surface in this study formed in a plane with capacitor current and output voltage error axises, so in such plane the steady state operating point will be the origin. Unfortunately formulation for forming the nonlinear switching surface is not explained clearly in the paper. As it is known, sensing the capacitor current is difficult and authors came up with a method to estimate the capacitor current, then the control algorithm formed based on that estimation. The control algorithm will move to non-linear

controller when the voltage error and current estimator exceed a threshold, then change the switch state after crossing the switching surface; and will move back to PID controller after the voltage error and capacitor current are near zero. Proposed method in this paper was applied on a buck converter and the nonlinear switching surface controller implemented as a Verilog HDL module. The key point of the non-linear controller was capacitor current estimation which enabled the switching surface evaluation. Using the estimation method helps to apply this method for actual systems even if the hardware for current sensing has low resolution. Since there is no explanation about how to form the switching surface, it is difficult to discuss the robustness of this method against modeling errors. However authors claimed that their method is robust and feasible for any dc-dc converter.

Meyer, Feng and Liu published three papers [34], [35] and [36], presenting their control algorithm for dc-dc converters based on the principle of capacitor charge balance. Their goal was to drive converters from load current variation or input voltage change to their steady state condition in optimum time. They based their algorithm on this principle; in steady state, the average of the capacitor current over one switching period must be equal to zero. In their study, four areas is defined between load current and the inductor current in a buck converter and the capacitor charge balance mapped on these areas. They took six steps to calculate these areas and find the switching times for the buck converter based on them. In the first step the new load current is estimated to avoid voltage drop at the output for large output current due to measurement. Inductor slew rate calculated in the second step through modeling the buck converter with its state equations. Step three is estimating the capacitor discharge portion which is one of those

mentioned areas. The first switching time and another portion of capacitor discharge is calculated in the fourth step, based on estimated load current and inductor current rising slew from steps one and two. In step five, the last portion of the capacitor discharge and the time which is needed for this discharge portion is estimated. The final step is calculating capacitor charge portion and finding the final switching times for the algorithm. Meyer and his colleagues claimed that these switching times is the minimum time required to move the converter to the steady state condition during a large load current change. The purposed algorithm may not work for a boost converter because in boost converters, load current and inductor current is completely separated while the switch is closed and the capacitor charge principle cannot be mapped on these currents. Another drawback of this algorithm is that modeling errors affect calculating the inductor current slew and capacitor discharging portions thus the calculated switching times might not be optimal.

In this chapter, theory of input shaping and time-optimal control reviewed and benefits and weaknesses of each method has been discussed. Utilizing Strength Pareto Evolutionary Algorithm (SPEA) to calculate a PID controller's gains for optimizing the settling time output overshoot has been reviewed. Since this a game theory algorithm, the final answer has acceptable settling time and overshoot but none of these properties of the system were minimized. Another approximate time-optimal method for dc-dc converters reviewed that was based on the capacitor current estimation. The last reviewed method was trying to find the time-optimal solution by using the capacitor state of charge in a buck converter.it is discussed that the presented method cannot be applied to dc-dc boost converters and it is sensitive to modeling errors.

In this study, a minimum-time optimal solution will be presented based on the system's total energy for dc-dc converters. The presented method will then applied on a dc-dc boost converter to drive from an initial state to reach a final state in minimum possible time. The simulation results confirm the ability of the proposed method in minimum-time optimal of the boost converter.

Chapter 3: Linear and Nonlinear Control of Dc-dc Converters

Boost converters are similar to any other dynamic system in case of stability or steady state errors. They should be designed in a way to have reasonable dynamic stability and following their input reference to minimize their steady state errors. Even in the well-designed systems, some huge disturbances can cause instability or losses in the system may cause some steady state errors in the outputs. Controllers are designed to compensate these problems. In this chapter, a boost converter is modeled and a linear stabilizing feedback controller is designed for the boost converter. A brief review and comparison between linear controllers and nonlinear controllers for boost converters is presented and benefits and drawbacks of each method are discussed.

3.1 Linear Control

Most of the systems in real word are non-linear, but since dealing with these systems are not easy, linearization methods have been developed to control the systems linearly near their operating point. Boost converters are also non-linear and need to be linearized to property design a linear control law. This linearization should be taken place near the boost converter desired operating point. After linearization and designing a linear controller for the boost converter, it will operate at the desired operation point and the controller will guaranty the stability of the converter and compensating small

disturbances. Sometimes linear controllers are not able to keep the stability of the system during large disturbances. As a simple and well-known example of linear controller, state feedback controllers are being used for linearized systems in many applications. It is possible to design them in such a way to have desired overshoot or undershoot with reasonable settling time, but in many applications they are not able to fulfill some constraints like very fast response.

3.1.1 Modeling of a Boost converter

Figure 3-1 shows a boost converter circuit schematic. To make the modeling easier and simplify the formulations, it is assumed that all semiconductor elements of the circuit are ideal. This means switch q_1 is loss less with infinitely fast response and the diode has zero volt threshold voltage.

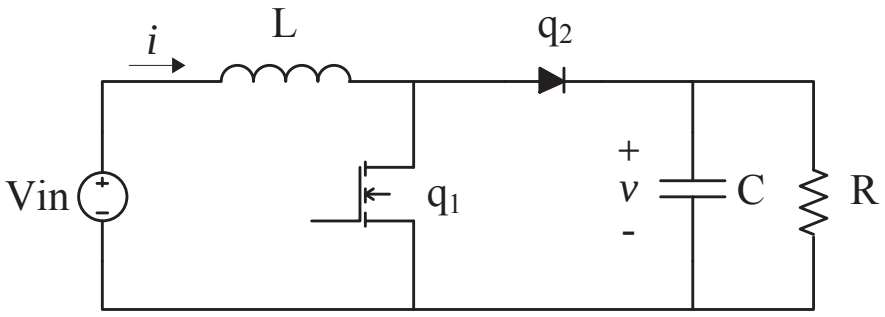

Figure 3-1: Switched dc-dc Boost converter with semiconductors

Based on the switch position, the boost converter may have two topologies: when the switch is on, diode q_2 is in non-conducting mode and as a result, source (V_{in}) and the load (R) are separated. Besides that, when the switch q_1 is open, the diode is forward bias and will conduct energy from the source to the load of the system R.

Figure 3-2 shows these two different topologies of the boost converter circuit.

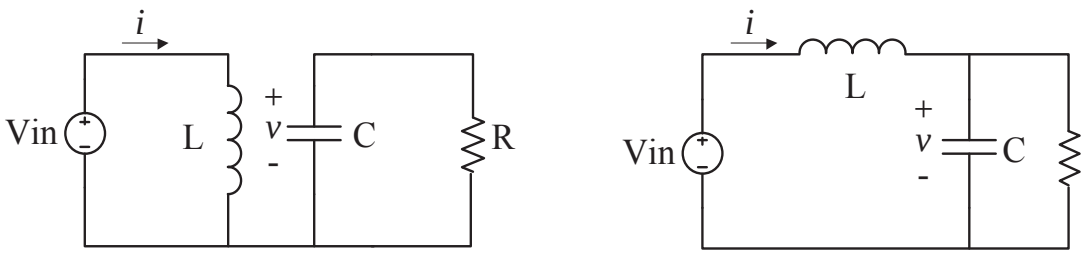

(a) switch *S* is close (b) switch *S* is open

Figure 3-2: Circuit topologies involved in the boost converter

To model the dynamic of the boost converter circuit, some numerical values should be defined to describe each circuit topology shown in Figure 3-2. In Figure 3-2(a) the converter circuit is shown when switch q_1 is closed. The numerical value $u = 1$ is attributed to this topology, while the numerical value $u = 0$ describes the second topology which is shown in Figure 3-2(b) where switch q_1 is open. A combination of the two circuits shown in Figure 3-2 is presented in Figure 3-3 to introduce the boost converter with ideal switch and ideal diode.

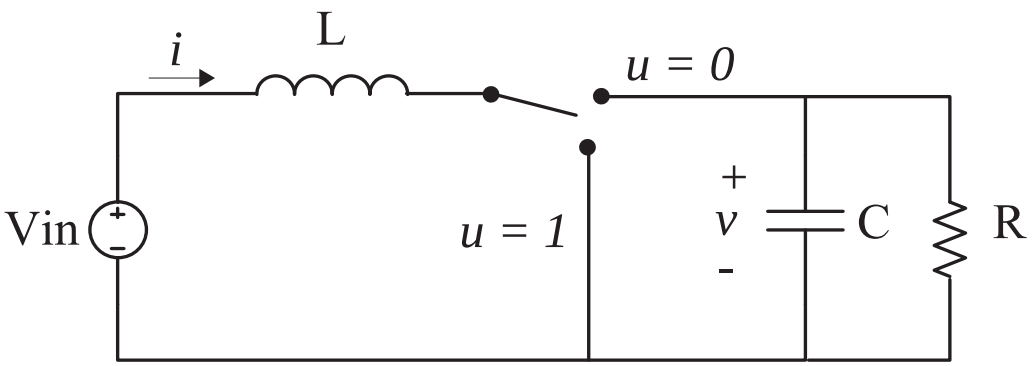

Figure 3-3: Boost converter after replacing the switch and diode with a two position switch

Kirchoff's laws may be applied to model the boost converter for each topology of the boost converter based on the condition of the switch. Following equations can be formed by applying Kirchoff's laws to the boost converter when $u = 1$

$$L\frac{di}{dt} = V_{in} \tag{3.1}$$

$$C\frac{dv}{dt} = -\frac{v}{R}\,. \tag{3.2}$$

Same approach of using the current and voltage law for the boost converter when switch q_1 is open yields

$$L\frac{di}{dt} = -v + V_{in} \tag{3.3}$$

$$C\frac{dv}{dt} = i - \frac{v}{R}. \tag{3.4}$$

The dynamics of the boost converter is formed by combining the above equations and including the switch position u as the input

$$L\frac{di}{dt} = -(1-u)v + V_{in} \tag{3.5}$$

$$C\frac{dv}{dt} = (1-u)i - \frac{v}{R}. \tag{3.6}$$

The system can be described as bilinear system [37], since the input and state variables linearly independent however the dynamics contain product of input and states of the form $x_i u$.

The boost converter system equations can be normalized as follow

$$\begin{pmatrix} x_1 \\ x_2 \end{pmatrix} = \begin{pmatrix} \frac{1}{V_{in}}\sqrt{\frac{L}{C}} & 0 \\ 0 & \frac{1}{V_{in}} \end{pmatrix} \begin{pmatrix} i \\ v \end{pmatrix} \tag{3.7}$$

where $x_1$and x_2 are inductor current and capacitor voltage respectively and with the normalized time

$$\tau = \frac{t}{\sqrt{LC}}.$$

Then the average model is

$$\frac{dx_1}{d\tau} = -(1-d_1)x_2 + 1 \tag{3.8}$$

$$\frac{dx_2}{d\tau} = (1-d_1)x_1 - \frac{x_2}{Q} \tag{3.9}$$

where d_1 represents the average input and $Q = R\sqrt{\frac{C}{L}}$.

Controlling a system may have different objectives such as stabilizing the output or tracking an input. In the dc-dc boost converter, stabilizing the capacitor voltage was the objective of the control design. In this case, it is needed to know the steady state behavior of the converter. The equilibrium points can be found by solving the system of equations (3.8) and (3.9), for steady state conditions which mean all the derivatives should set to be zero and the control input assume to have constant value.

Steady state system of equations in matrix form is then

$$\begin{pmatrix} 0 & (1-d_1) \\ (1-d_1) & -\frac{1}{Q} \end{pmatrix} \begin{pmatrix} \overline{x_1} \\ \overline{x_2} \end{pmatrix} = \begin{pmatrix} 1 \\ 0 \end{pmatrix} \quad 3.10$$

The steady states values $\overline{x_1}$ and $\overline{x_2}$ can be found by solving the system of equations (3.10) [37]

$$\overline{x_1} = \frac{1}{Q} \frac{1}{(1-d_1)^2} \quad 3.11$$

$$\overline{x_2} = \frac{1}{(1-d_1)}. \quad 3.12$$

To describe the obtained equilibrium points where the output voltage considered as set point V_d, parameter $\overline{x_2}$ should be changed to V_d and the equilibrium point with new parameter would be

$$\overline{x_1} = \frac{1}{Q} V_d^2$$

$$\overline{x_2} = V_d$$

$$d_1 = \frac{V_d - 1}{V_d}.$$

Transfer function of the boost converter after normalization can be obtain from relations (3.11) and (3.12) as follow

$$H(D) = \overline{x_2} = \frac{1}{(1 - d_1)}. \qquad 3.13$$

Since the average control input d_1 (Duty Cycle) is limited between zero and one, the boost converter's gain is always greater than one. Output voltage gain of the boost converter in terms of the control input is shown in Figure 3-4.

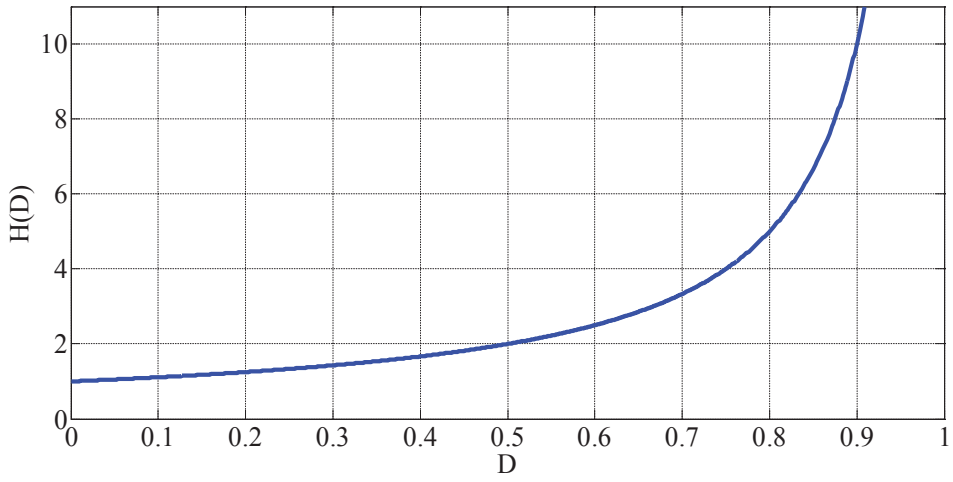

Figure 3-4: Output voltage gain of the boost converter in terms of the control input

Equilibrium points for the boost converter without linearization can obtain as

$$\bar{\imath} = \frac{1}{R}\frac{\bar{v}^2}{V_{in}} \quad , \quad \bar{v} = \frac{V_{in}}{(1-d_1)}. \tag{3.14}$$

Generally it is assumed that the value $u = 1$ shows the condition that switch q_1 is on and $u = 0$ shows the condition which the switch is off. Sometimes to simplify the modeling and formulation, an alternative model can be used like

$$\frac{dx_1}{d\tau} = -d_2 x_2 + 1 \tag{3.15}$$

$$\frac{dx_2}{d\tau} = d_2 x_1 - \frac{x_2}{Q} \tag{3.16}$$

where

$$d_2 = 1 - d_1. \tag{3.17}$$

New state equilibriums would be

$$\bar{x}_1 = \frac{V_d^2}{Q} \quad and \quad \bar{u}_{av} = \frac{1}{V_d}.$$

A dc-dc boost converter modeled and normalized in this chapter. The alternative model for the boost converter is presented in (3.15) and (3.14). This alternative model makes the linearization's formulation simpler.

3.1.2 Approximate Linearization

Linearized average state system model of (3.15) and (3.16) around (3.14) is [37]

$$\dot{x}_{1\delta} = -\frac{1}{V_d} x_{2\delta} - V_d u_{av,\delta} \tag{3.18}$$

$$\dot{x}_{2\delta} = \frac{1}{V_d} x_{1\delta} - \frac{1}{Q} x_{2\delta} + \frac{V_d^2}{Q} u_{av,\delta} \tag{3.19}$$

where

$$x_{1\delta} = x_1 - \frac{V_d^2}{Q}$$

$$x_{2\delta} = x_2 - V_d$$

$$u_{av,\delta} = d_2 - \frac{1}{V_d}.$$

Linearized average state system model in matrix form, $\dot{x}_\delta = Ax_\delta + Bu_{av,\delta}$, is

$$\dot{x}_\delta = \begin{bmatrix} 0 & -\frac{1}{V_d} \\ \frac{1}{V_d} & -\frac{1}{Q} \end{bmatrix} x_\delta + \begin{bmatrix} -V_d \\ \frac{V_d^2}{Q} \end{bmatrix} u_{av,\delta}. \tag{3.20}$$

Prior to design a controller for dynamic system, it is necessary to know if it is possible to control the system or not (controllability); or if it is possible to determine the states of the system from its outputs (observability). Controllability and observibility matrices are defined [38] to check these properties of a system. The system is controllable if its controllability matrix has full rank and the same law is also applied for observability.

The controllability matrix of the linearized system of (3.20) is

$$C = \begin{bmatrix} -V_d & -\frac{V_d}{Q} \\ \frac{V_d^2}{Q} & -(1+\frac{V_d^2}{Q^2}) \end{bmatrix}.$$

Rank of a 2x2 matrix can be verified through its determinant, if the matrix determinant is nonzero then the matrix has full rank. Determinant of the above controllability matrix is

$$\det C = V_d(1+2\frac{V_d^2}{Q^2})$$

which is not zero, so the system (3.20) is controllable. Two observability matrices could be formed depends on, which state is selected as output, so when $y_\delta = x_{2\delta}$ the observability matrix is

$$O = \begin{bmatrix} 0 & 1 \\ \frac{1}{V_d} & -\frac{1}{Q} \end{bmatrix}$$

and

$$\det O = -\frac{1}{V_d},$$

so the system is observable in this case. Similarly, when $y_\delta = x_{1\delta}$ the observability matrix is

$$O = \begin{bmatrix} 1 & 0 \\ 0 & -\frac{1}{V_d} \end{bmatrix}$$

and

$$\det O = -\frac{1}{V_d},$$

observability of the system is proofed for this case as well. Since the system found controllable and observable, state feedback controller can be designed for it.

3.1.3 Control via State Feedback

Different linear methods are developed and utilized to control the boost converter near desired equilibrium point. State feedback control technique is presented in this section as an example of linear controller for dc-dc boost converter. It is shown that the system of (3.18) and (3.19) is controllable and observable; as a result it can be stabilized by using linear state feedback. The feedback controller is

$$u_{av,\delta} = -k_1 x_{1\delta} - k_2 x_{2\delta}. \tag{3.21}$$

The average closed loop system obtained from the state feedback controller (3.21) is presented in matrix form

$$\dot{x}_\delta = \begin{bmatrix} k_1 V_d & -\left(\frac{1}{V_d} - k_2 V_d\right) \\ \left(\frac{1}{V_d} - k_1 \frac{V_d^2}{Q}\right) & -\left(\frac{1}{Q} + k_2 \frac{V_d^2}{Q}\right) \end{bmatrix} x_\delta. \tag{3.22}$$

The characteristic polynomial of the average closed loop boost converter is found to be [37]

$$p(s) = s^2 + \left(\frac{1}{Q} + k_2\frac{V_d^2}{Q} + k_1 V_d\right)s + \frac{1}{V_d^2} - k_2 - 2k_1\frac{V_d}{Q}. \quad 3.23$$

Gains for the state feedback controller can be found by equating the equation (3.23) and the desired traditional characteristic polynomial form $p_d(s) = s^2 + 2\zeta\omega_n s + \omega_n^2$,

$$k_1 = \frac{1}{V_d\left(1 - \frac{2V_d^2}{Q^2}\right)}\left[-\frac{2}{Q} + 2\zeta\omega_n + \frac{V_d^2}{Q}\omega_n^2\right] \quad 3.24$$

$$k_2 = -\frac{1}{V_d\left(1 - \frac{2V_d^2}{Q^2}\right)}\left[\frac{2V_d}{Q}\left(-\frac{1}{Q} + 2\zeta\omega_n\right) + V_d\left(\omega_n^2 - \frac{1}{V_d^2}\right)\right]. \quad 3.25$$

A state feedback controller designed for the linearized model of a dc-dc boost converter and the closed loop gains are calculated. Pole placement method also can be used to find the controller parameters ζ and ω_n values and then come up with state feedback gains.

3.2 Nonlinear Control

It is true that linear control is widely used in industries and helped engineers for this great movement during past decades in automation; but there are many reasons that researchers are highly interested in development and applications of nonlinear control such as Feedback Linearization, Gain Scheduling, Lyapunov Redesign and Sliding Mode. Some of the reasons are: improvement of existing control systems, analysis of hard nonlinearities, dealing with model uncertainties, design simplicity and cost and performance optimality. To explain some of these reasons, linear controllers in some applications require very accurate and high quality sensors to gather correct and enough

information for controller as well as high quality actuators to produce linear behavior [39]. However less expensive devices can be used in nonlinear controller because they can handle nonlinearity behaviors. On the other hand, as it is mentioned previously, linear controllers are assumed to be used in small range of operation and when the operation range is larger, linear controllers might not be able perform well; nonlinear controllers are able to handle wide range of nonlinearity in the system operation. Optimal performance is one of the most famous reasons that researchers are interested to develop and improve the nonlinear control methods. All the studies that have been reviewed in Chapter 2 were nonlinear control. Nonlinear systems are harder to analyze but it doesn't mean that designing a nonlinear controller is always harder to formulate or apply to a system. Boost converters are nonlinear systems but they can be linearized and controlled easily it is shown in Section 3.1 . This study aims to introduce and develop a method to control a boost converter during load change in minimum time. As it is mentioned above, nonlinear control techniques are stronger to offer performance optimality. Bang-bang control is one of the control techniques with fastest settling time which is inherently nonlinear and is the base idea for the method which will be developed in this study and will be presented in the next chapter.

Chapter 4: Time-Optimal Control

In this chapter, theory of the problem and the innovated solutions is discussed. A boost converter is modeled and its state equations are presented. A nonlinear controller which is designed to drive the boost converter from an initial state to a final state is introduced. Simulation and the results of study are presented.

4.1 Bang-Bang Control

The problem is driving a boost converter from an initial operating point to a final operating point in the fastest possible time. If the boost converter is designed to have stable poles, it can move between short ranges of states and remain stable, without any controller. This way of changing the operation point is not fast, and might have huge overshoot or undershoot. Figure 4-1 shows step response of a boost converter that didn't have any controller. As it is shown in the figure, the output voltage has about 0.01 s settling time and more than 10% overshoot.

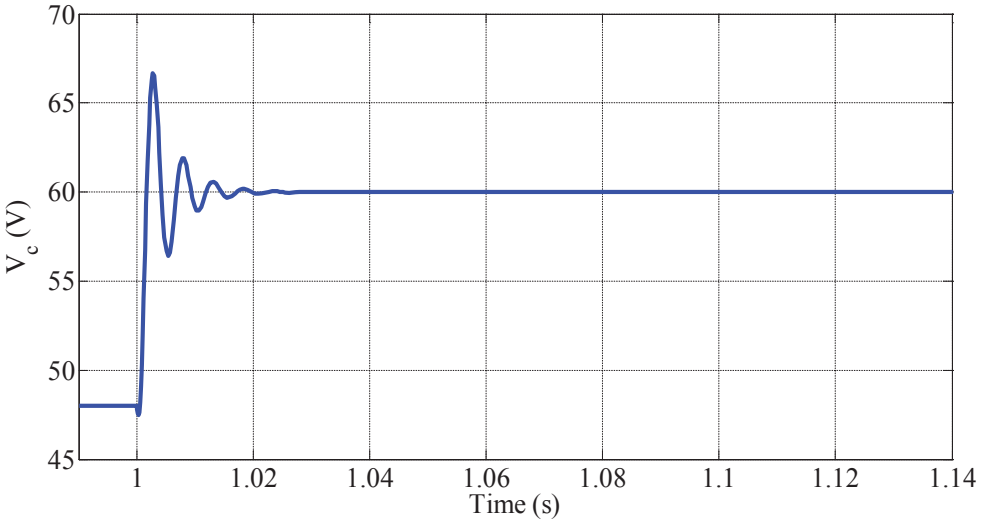

Figure 4-1: Output voltage of a boost converter with no controller after a step change in duty cycle

Controllers can be designed to reduce the overshoot or settling time of the system. A PI controller is designed to show its effect on dynamic response of the dc-dc boost converter. Three different sets of gains are utilized in the boost converter to compare the effects of gains on the capacitor voltage. Gain values are presented in Table A.

Table A: Different gain values for PI controller

Gain Set 1	$k_P = 1.0 \times 10^{-6}$ $k_I = 4.0 \times 10^{5}$	Settling time: 0.05 s Overshoot: 0.0 %
Gain Set 2	$k_P = 2.0 \times 10^{-6}$ $k_I = 5.0 \times 10^{5}$	Settling time: 0.018 s Overshoot: 0.0 %
Gain Set 3	$k_P = 5.5 \times 10^{-6}$ $k_I = 5.0 \times 10^{5}$	Settling time: 0.007 s Overshoot: 1.4 %

Capacitor voltage of dc-dc boost converter for different gain values of PI controller is shown in Figure 4-2. For set 1, the capacitor voltage is overdamped which caused a long settling time for the system. Set 2 is critically damped and the capacitor voltage has no overshoots while the settling time is still longer than the step response of the

system without PI controller. To decrease the settling time, proportional gain of the controller is increased in set 3, the capacitor voltage has a fast settling time with an overshoot of less than 1%. As it is discussed in Chapter 2, there is a trade-off between increasing the settling time and decreasing the overshoot of the system. Since the gains in PI controller are limited [40], it is not possible to get the minimum-time response with PI controllers.

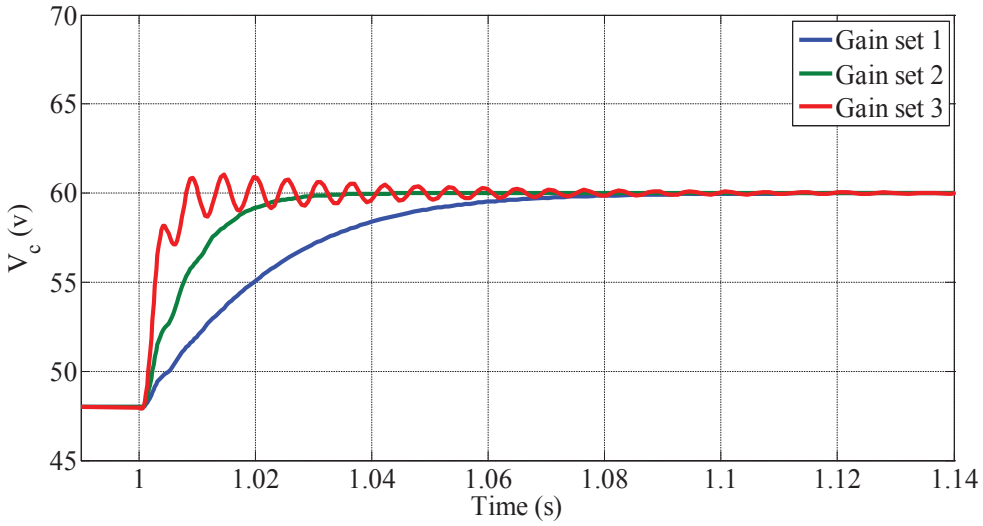

Figure 4-2: Output voltage for a boost converter with PI controller

All systems move between different states through their trajectories in the state space. Trajectories for each system depend on the system properties and system input as well. When the boost converter moves to the new operating point with changing its duty cycle, it means after that the duty cycle is changed; boost converter starts traveling on the new trajectory to reach the new state. As it is shown in Figure 4-3, by changing the duty cycle, phase plane portrait will change to the red one. System was working at point

a, then by changing the duty cycle, operation point will start traveling through the black path to reach the point b which is its new operation point.

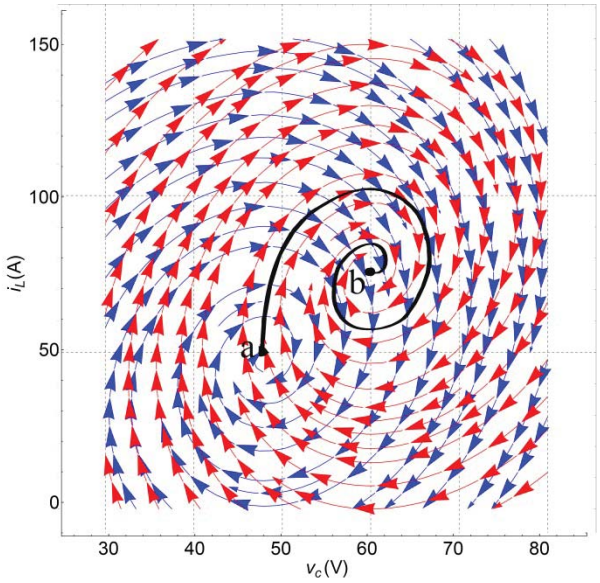

Figure 4-3Boost converter phase plane portrait in average mode for u=0.5 (blue) and u=0.6 (red)

To have the fastest transition between the two operating points, the boost converter should be driven on its fastest trajectory. Control inputs are limited in all systems, so the fastest time to travel between the two states is also limited. In bang-bang control the boost converter is driven with its input limits and with only one switch, the boost converter will reach to the desired final state. The most important and challenging part of this bang-bang method, is calculating the switching time to achieve the fastest transient time. For a system with state equations shown in (4.1) and input limits of (4.2), bang-bang control formulations are

$$\dot{x} = f\big(t, x(t)\big) + g\big(t, x(t)\big)u(t) \tag{4.1}$$

$$a \leq u \leq b. \tag{4.2}$$

Objective function for minimizing the time and Hamiltonian equation are presented in equations (4.3) and (4.4) respectively [41].

$$J(x) = \theta[x(t), t]|_{t_0}^{t_f} + \int_{t_0}^{t_f} (\emptyset[x(t), t] + u(t)h[x(t), t])\, dt \tag{4.3}$$

$$H = \emptyset(x(t), t) + u(t)h(x(t), t) + \lambda(t)\left(f\big(t, x(t)\big) + g\big(t, x(t)\big)u(t)\right). \tag{4.4}$$

From the minimum principle, the solution is

$$\partial_{u(t)}H = 0 = h(x(t), t) + \lambda(t)g\big(t, x(t)\big). \tag{4.5}$$

However this solution is not a function of control input and cannot be solved directly for $u(t)$, as it is bang-bang control, the input limits (4.6) can be enforced to the solution and find the co-state solution (4.7).

$$u(t) = \begin{cases} a & if \quad h(x(t), t) + \lambda(t)g\big(t, x(t)\big) > 0 \\ b & if \quad h(x(t), t) + \lambda(t)g\big(t, x(t)\big) < 0 \end{cases} \tag{4.6}$$

$$\partial_{x(t)}H + \dot{\lambda}(t) = 0. \tag{4.7}$$

Co-state solution has the following boundary constraints

$$\big(\partial_{x(t)}\theta[x, t] - \lambda\big)|_{t_0}^{t_f} = 0. \tag{4.8}$$

For solving the above problem in MATLAB or Mathematica, t_0 and t_f should be known parameters, however terminal time t_f is unknown. To solve this issue, the time scale can be changed to

$$t = T_f \tau.$$

By taking $\tau \in [0,1]$ and the parameter T_f as a scaling factor, any time range $t \in [0, T_f]$ can be calculated. After these changes, time differential will change to $dt = T_f d\tau$ and another state equation will be added to the system of equations

$$\frac{dT_f}{d\tau} = 0.$$

The bang-bang control method and the time scaling technique is applied to a boost converter showed in Figure 3-1. Parameters for the boost converter are presented in Table B.

Table B: Boost converter parameters

Parameter	***Value***
V_{in}	24 V
L	0.1 mH
C	1000 µF
R	2 Ω

The converter is driven from initial condition $v_c(0) = 48\,V$ and $i_L(0) = 48\,A$ to the final operation point of $v_c(t_f) = 60\,V$ and $i_L(t_f) = 75\,A$. The state equations for the converter are

$$\frac{di_L(t)}{dt} = \frac{1}{L}(V_{in} - (1-q)v_c(\mathrm{t})) \qquad 4.9$$

$$\frac{dv_c(t)}{dt} = \frac{1}{C}\left((1-q)i_L(t) - \frac{v_c(t)}{R}\right). \qquad 4.10$$

Objective function is

$$J = (i_L(t_f) - i_{Lf})^2 + (v_c(t_f) - v_{cf})^2 + \int_0^{t_f} 1\, dt. \quad 4.11$$

As it is mentioned before, there is not any direct way to find t_f in the above equations. Since this is a free time problem, the time is scaled and the state equations are changed to

$$\frac{di_L(\tau)}{d\tau} = \frac{1}{L} T_f (V_{in} - (1-q) v_c(\tau)) \quad 4.12$$

$$\frac{dv_c(\tau)}{d\tau} = \frac{1}{C} T_f \left((1-q) i_L(\tau) - \frac{v_c(\tau)}{R} \right). \quad 4.13$$

New objective function after the changes is

$$J = (i_L(1) - i_{Lf})^2 + (v_v(1) - v_{cf})^2 + \frac{1}{2} {T_f}^2. \quad 4.14$$

This system of equations can be solved with the same procedure that presented in equations (4.1) to (4.8). MATLAB or Mathematica can be used to get the numerical result. NDSolve command of Mathematica is used to solve the problem, but some problems might be happen while using NDSolve because some initial and final values are known in the boundary values. Shooting method in Mathematica is used to overcome this problem.

After solving the problem, the total minimum time is 0.00062085 s. As it is mentioned above, for a second order system only one switching is needed during this minimum time period. This switching time can be easily found by finding the minimum point of v_c and it is 0.000383293 s. The phase plane portrait of the boost converter during bang-bang control is shown in Figure 4-4. Green lines present the boost converter trajectory

when the switch q_1 is conducting and yellow lines are the boost converter trajectory when the switch is open.

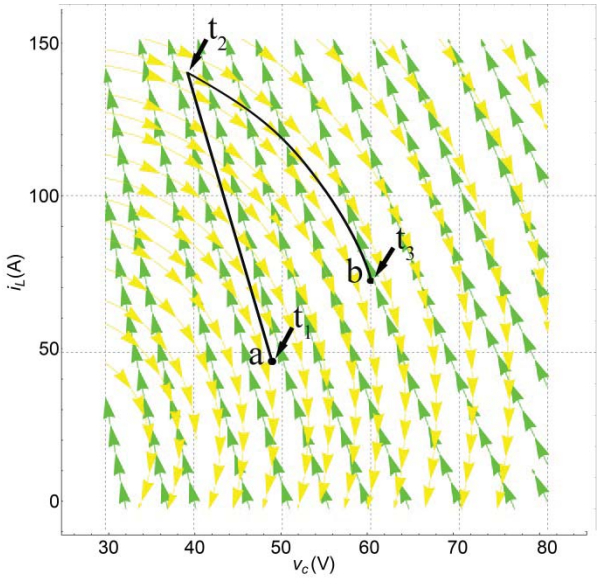

Figure 4-4: Boost converter phase plane portrait when q=1 (green) and q=0 (yellow)

Point (a) in Figure 4-4 is the initial operating point of the converter, during the bang-bang control converter traveled through the black path to reach the point (b) which is its desired final operating point. Capacitor voltage of the average mode boost converter during bang-bang control is shown in Figure 4-5, in comparison with the settling time of 0.01 for PI controller, the bang-bang control is much more faster.

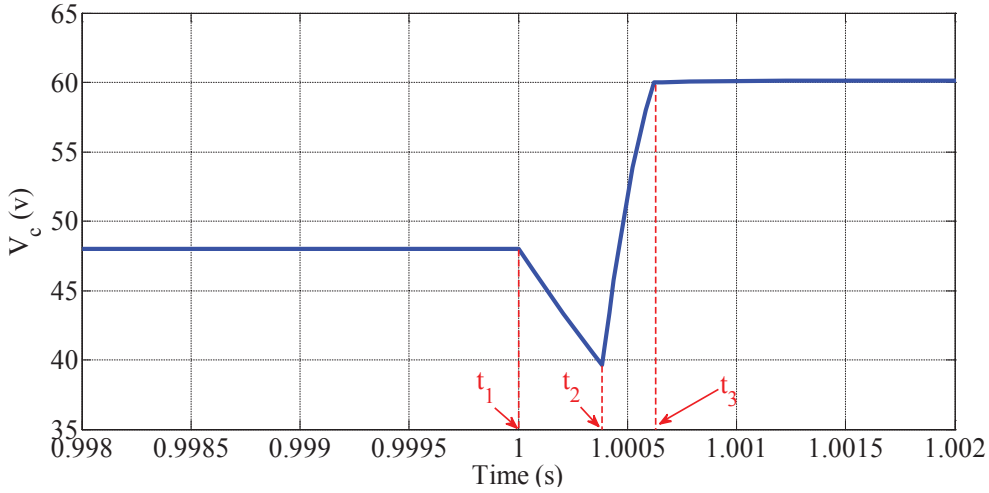

Figure 4-5: Capacitor voltage of the average mode boost converter during bang-bang control

The inductor current for average mode boost converter is shown in Figure 4-6, inductor current is the other state of the system which is changed during the bang-bang control. At first period that the switch is on, inductor current increased and after that the switch position changed went down to reach its final value.

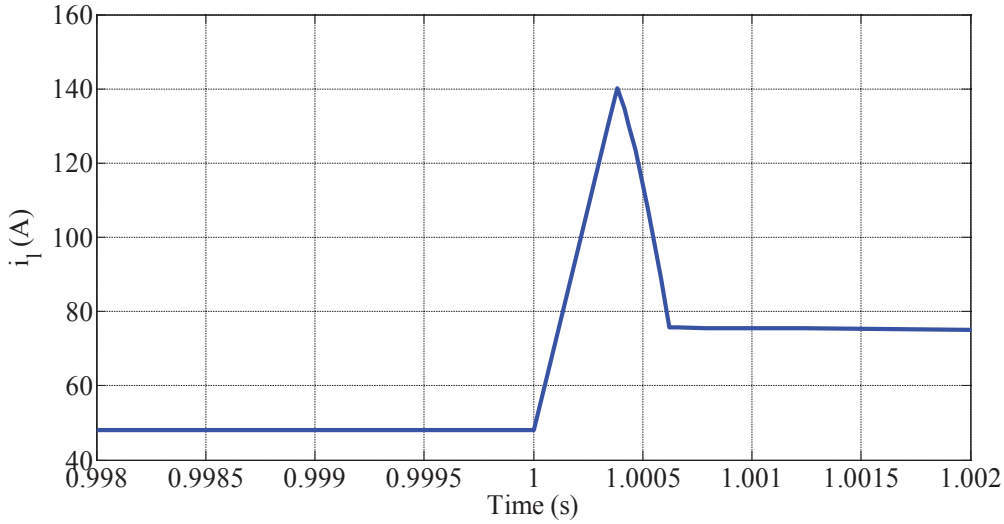

Figure 4-6: Inductor current of the average mode boost converter during bang-bang control

Same switching time can be applied to the switched mode boost converter model. Capacitor voltage for switched mode boost converter during bang-bang control is shown in Figure 4-7, and a very low frequency oscillation is seen for voltage as a result of switching.

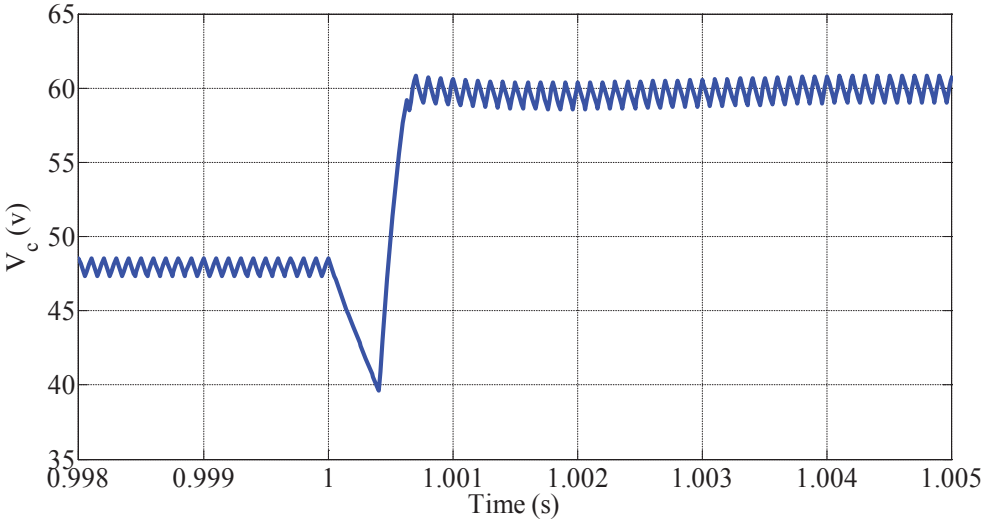

Figure 4-7: Capacitor voltage of the switched mode boost converter during bang-bang control

Same oscillation is seen for the inductor current in Figure 4-8.

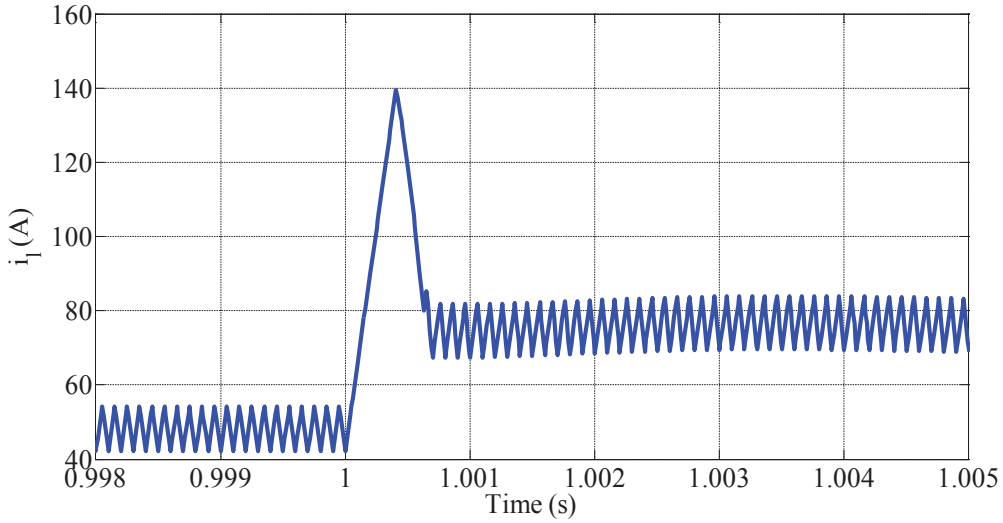

Figure 4-8: Inductor current of the switched mode boost converter during bang-bang control

Operation regions for control input in the switched mode simulation is

$$q = \begin{cases} PWM\ D = 0.5 & if \quad t < 1\ s \\ \begin{cases} 1 & if\ \ t < 0.000383293\ s \\ 0 & if\ \ t \geq 0.000383293\ s \end{cases} & if \quad 0 \leq t < 0.00062085\ s. \\ PWM\ D = 0.6 & if \quad t \geq 0.00062085\ s \end{cases}$$

Theory of bang-bang controller and time optimization problem are presented in this section. As it is obvious, the presented method is an open loop solution and is not suitable to apply to actual systems. A novel close-loop solution will be introduced in the next section.

4.2 Energy Based Closed Loop Method

The most important part of a closed loop system is feedback signals which give information about the present state of the system. This information helps the controller

to drive the system to the desired final operating point. In the boost converter, capacitor voltage, inductor current and load current are available variables to measure. This study is aimed to optimize the time response of a boost converter, having the time as the objective variable besides current and voltage as feedback variables makes it difficult to have a feedback loop. System's energy is another variable which can be calculated throw the current and voltage during the time. An Energy based method has been presented in [42] for dc-dc boost converters and another one for buck converters in [43] but none of them is time-optimal. So looking at the energy of the system makes it possible to have a relationship between the objective variable of the problem and actual feedback information from the boost converter.

During the bang-bang control, control input, is 1 for the first portion of the period and is 0 for the rest of the period. It means that switch q_1 in Figure 3-1 is closed in the first portion of bang-bang control and is open in the second portion. The boost converter circuit for these two situations is shown in Figure 3-2. As it is shown in Figure 3-2 (a), in the first period of bang-bang control, the inductor *L* is gaining energy from the source and capacitor's energy is dissipating in the load. Differential equations of the system in this period are

$$\frac{di_L}{dt} = \frac{1}{L} V_{in} \tag{4.15}$$

$$\frac{dv_c}{dt} = \frac{1}{C}\left(-\frac{v_c}{R}\right). \tag{4.16}$$

Forming the A matrix for system above considering i_l and v_c as system's states is

$$A = \begin{bmatrix} 0 & 0 \\ 0 & -\frac{1}{RC} \end{bmatrix}$$

and eigenvalues of the circuit in this condition are

$$\lambda_1 = 0 \quad and \quad \lambda_2 = -\frac{1}{RC}.$$

As it is shown, the system has zero eigenvalue in this topology which shows instability of the system during the time that the switch is closed. Considering the inductor's resistance in the equations eliminate the zero eigenvalue and move the eigenvalues to the left hand side of state space plane. The boost converter circuit schematic with considering the inductor's resistance is shown in Figure 4-9 during the time that the switch is closed.

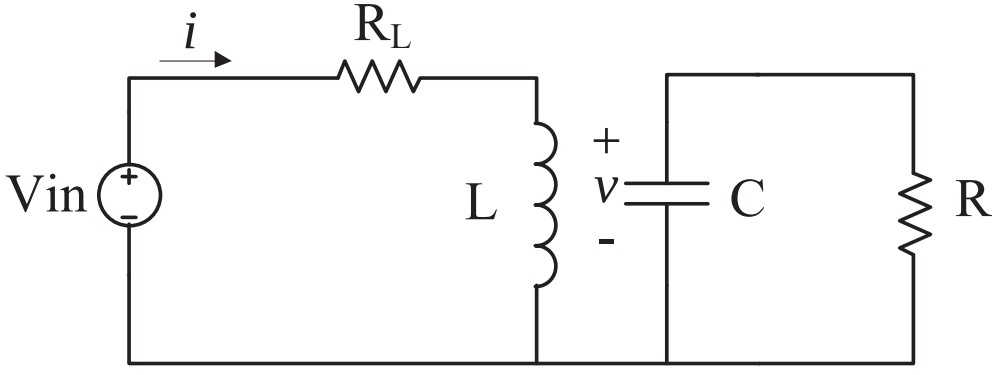

Figure 4-9: Boost converter when the switch is on with inductor's resistance

Differential equations for this topology are

$$\frac{di_L}{dt} = \frac{1}{L}(V_{in} - R_L i_L) \quad 4.17$$

$$\frac{dv_c}{dt} = \frac{1}{C}\left(-\frac{v_c}{R}\right). \quad 4.18$$

The new A matrix for the system considering i_l and v_c as system's states is

$$A = \begin{bmatrix} \frac{-R_L}{L} & 0 \\ 0 & -\frac{1}{RC} \end{bmatrix}$$

and new eigenvalues are calculated as

$$\lambda_1 = -\frac{R_L}{L} \quad and \quad \lambda_2 = -\frac{1}{RC}.$$

In this case both eigenvalues are negative and the system is stable. Considering this resistance for the inductor helps modeling to be more accurate to match the real circuit. In the second period, circuit acts like a RLC circuit and capacitor gaining energy from both the inductor and the source and the differential equations for the system are

$$\frac{di_L}{dt} = \frac{1}{L}(V_{in} - v_c) \quad 4.19$$

$$\frac{dv_c}{dt} = \frac{1}{C}\left(i_L - \frac{v_c}{R}\right). \quad 4.20$$

To investigate the stability of the system in this condition, the A matrix of the system is formed assuming i_l and v_c as system's states

$$A = \begin{bmatrix} 0 & -\frac{1}{L} \\ \frac{1}{C} & -\frac{1}{RC} \end{bmatrix}$$

and the eigenvalues are

$$\lambda_{1,2} = \frac{-L \mp \sqrt{L^2 - 4LCR^2}}{2RLC}.$$

It is clear that the eigenvalues of this topology has negative real part for all amounts of the parameters. As a result the system is stable at this condition.

The overall energy flow in the boost converter can be divided into two periods depending on the switch position in the circuit. These two topologies of the boost converter are shown and the stability of the system is discussed. In the energy flow point of view, when the switch is on, inductor energy starts increasing and energy flows to the inductor from the source. At the same time, the stored energy in the capacitor is dissipating in the load. These energy conversions are totally independent while the switch is closed. During this time the amount of energy which builds up in the inductor is

$$\Delta W_{L1} = \frac{1}{2} L\left(i_L^2(t_2) - i_L^2(t_1)\right) \qquad 4.21$$

and this energy comes from the source. At the same time, the energy of capacitor discharges into the load

$$\Delta W_{C1} = \frac{1}{2} C\left(v_C^2(t_2) - v_C^2(t_1)\right) \qquad 4.22$$

where t_1 and t_2 shown in Figure 4-5 and are the start time of bang-bang control and the switching time respectively. From Figure 4-5 and Figure 4-6 it is seen that

$$i_L(t_2) > i_L(t_1)$$

$$and\ v_C(t_2) < v_C(t_1),$$

as a result

$$\Delta W_{L1} > 0$$

$$and\ \Delta W_{C1} < 0$$

which means stored energy of the inductor is increasing and the stored energy in the capacitor is decreasing. Figure 4-10 shows the energy flow in the circuit while the switch is on.

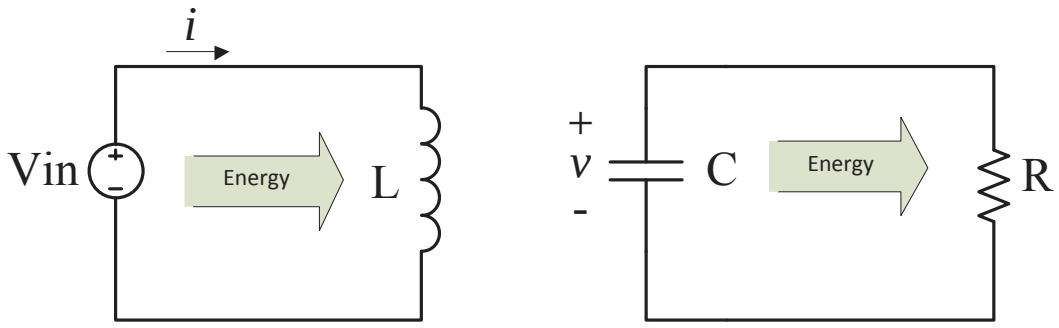

Figure 4-10: Energy flow in the boost converter circuit while the switch q_1 is closed

The other time period is during the time that switch q_1 is open and all the components of the boost converter are electrically connected. During this period, energy flows to the capacitor from both the inductor and the source while at the same time, some portion of the energy that coming from the inductor and the source is dissipating in the resistor. During this time period, amount of the stored energy in the inductor is decreased as

$$\Delta W_{L2} = \frac{1}{2} L\left(i_L^2(t_3) - i_L^2(t_2)\right) \qquad 4.23$$

and at the same time, the energy of capacitor increases as

$$\Delta W_{C2} = \frac{1}{2} C\left(v_C^2(t_3) - v_C^2(t_2)\right). \qquad 4.24$$

The energy flow during this period is shown in Figure 4-11.

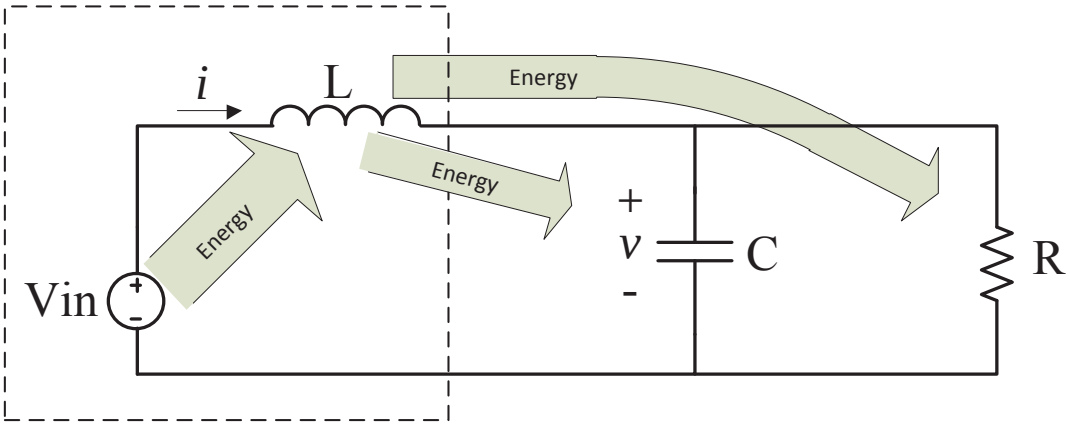

Figure 4-11: Energy flow in the boost converter circuit while the switch q_1 is off

Amount of energy which can be stored in the inductor is limited because the inductor current is limited and the inductor's core might be saturated for large currents as well [44]. As a result the inductor's participation in charging the capacitor while the switch is on is limited. On the other hand, total energy stored in the system (inductor and capacitor together) is changing when the converter's state changes

$$\Delta W_T = \frac{1}{2} C\left(v_C^2(t_3) - v_C^2(t_1)\right) + \frac{1}{2} L\left(i_L^2(t_3) - i_L^2(t_1)\right) \qquad 4.25$$

where ΔW_T is the total energy change in the system.In this case (moving to an operating point with higher voltage), the total amount of energy is increasing because both

inductor current and capacitor voltage is increasing. By looking at the relationship between the total energy change in the system and the ratio of inductor energy that participate in charging the capacitor, to the amount of energy that added to the inductor in the first period of bang-bang control

$$\beta = \frac{|i_L^2(t_3) - i_L^2(t_2)|}{|i_L^2(t_2) - i_L^2(t_1)|} \times 100 \qquad 4.26$$

where β is the inductor energy ratio. It is seen that by increasing the total energy change of the system, the participation of inductor in charging the capacitor is decreased. Figure 4-12 shows this relationship.

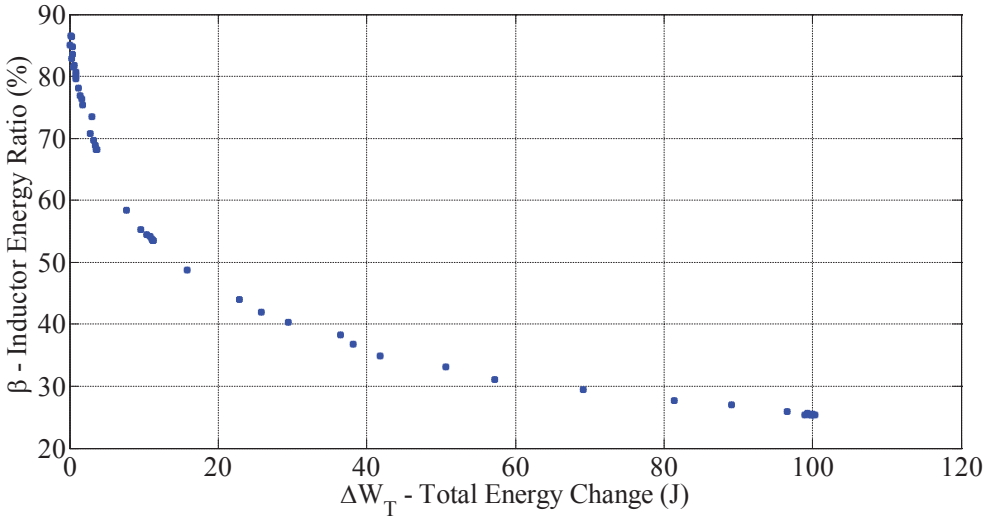

Figure 4-12: Relationship between Inductor Energy Ratio and Total Energy Change of the System

The information for forming Figure 4-12 is gathered by running the open-loop time optimal algorithm for calculating bang-bang control switching time which is presented in previous section for different scenarios on the ideal model of boost converter

presented in Figure 3-1. Data and simulation are presented in Appendix A and Appendix B respectively. By fitting a curve on the points of Figure 4-12, an energy based switching surface can be produced to use for close-loop control of boost converter in minimum time. MATLAB "cftool" is used to obtain the switching surface and the curve fitting result is shown in Figure 4-13.

The rational function for the fitted curve in Figure 4-13 is

$$\beta = \frac{-0.1008\,\Delta W_T^2 + 30.32\,\Delta W_T + 706.2}{\Delta W_T + 8.226}. \qquad 4.27$$

Equation 4.27 is used to form the close loop controller for the boost converter.

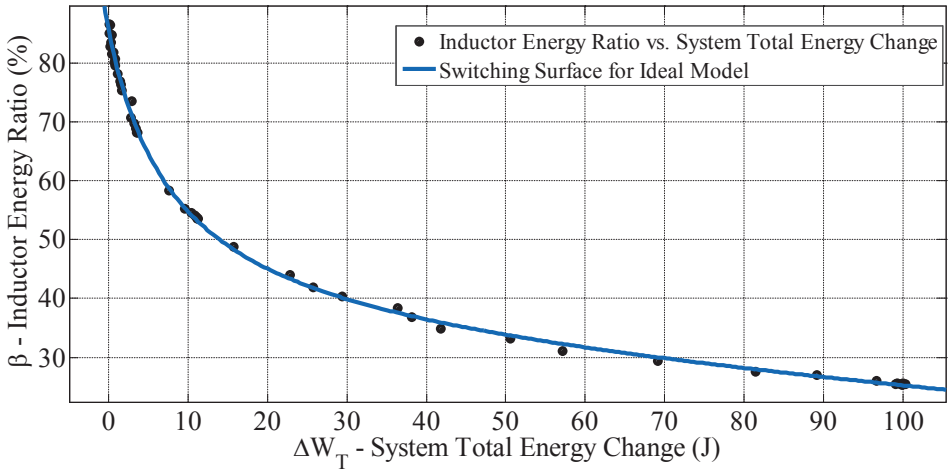

Figure 4-13: Switching Surface for Ideal Model of the System

The close loop control algorithm contains three main steps to perform the bang-bang control for the boost converter. In the first step, the change of total energy stored in the system after driving to the final operation point is calculated and the inductor energy ratio is determined by using equation 4.27. In the second step, switch q_1 in the boost

converter of Figure 3-1 will be closed until the inductor energy reaches the calculated value in step 1. In the final state, switch q_1 will be open until the capacitor voltage reaches to its value in the final state, after that the converter will continue its normal operation with the new duty cycle to remain in the new operating point.

The main challenge in the time optimal bang-bang control of the boost converter was calculating the switching times which has discussed in the previous section, in this section an energy based method presented that makes it possible to have close loop control for the time optimal bang-bang control of the boost converter. The first switching time which was founded by maximum value of the inductor current in the previous section is changed to finding the energy ratio of the inductor. The final switching time which was the optimal time calculated with minimization method is replaced by measuring the capacitor voltage to figure out reaching the final operating point. Equivalency of first switching time and the inductor energy ratio is discussed; equivalency of reaching the capacitor voltage to the desired voltage at the new operating point and the final switching time can be proved based on this fact that the trajectory of boost converter with the control input equals to 0 is unique. So if the converter starts traveling on this trajectory from the correct point (t_2), it will definitely reach the desired operating point; the desired operating point can be recognized through the capacitor voltage value or the inductor current.

4.3 Simulation and Results

4.3.1 Simulation

The boost converter of Figure 3-1 is modeled in MATLAB\Simulink. MATLAB code and Simulink block diagram presented in Appendix C. All possible losses and parasitic components are modeled to obtain the most accurate results. The boost converter circuit schematic is shown in Figure 4-14 including all parasitic elements and losses. In addition to the elements shown in the schematic, N-channel MOSFET from Simscape library is utilized in the MATLAB\Simulink simulation and modified with the detailed properties of a real MOSFET with part number TK72A08N1 which some of its important parameters presented in Table C.

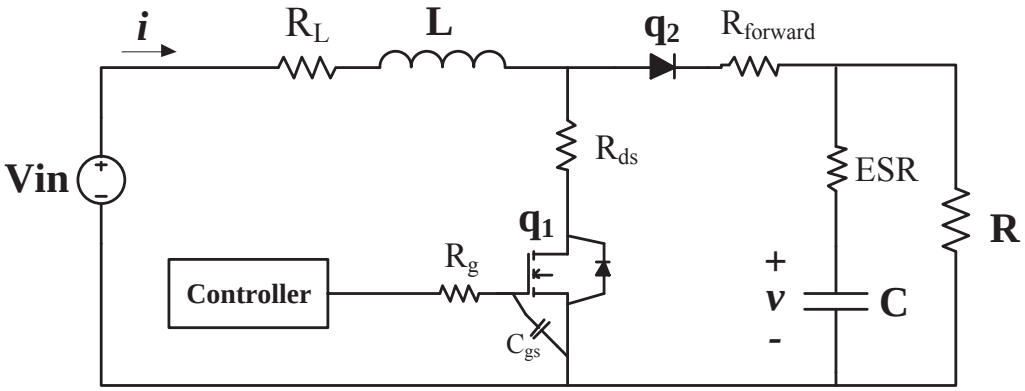

Figure 4-14: Boost converter Circuit with parasitic elements

Since parasitic parameters and elements added to the model, some properties of the simulated circuit is changed and the switching surface of Figure 4-13 is changed for the

detailed model. Comparison between the ideal model data set and the detailed model data set is presented in Figure 4-15.

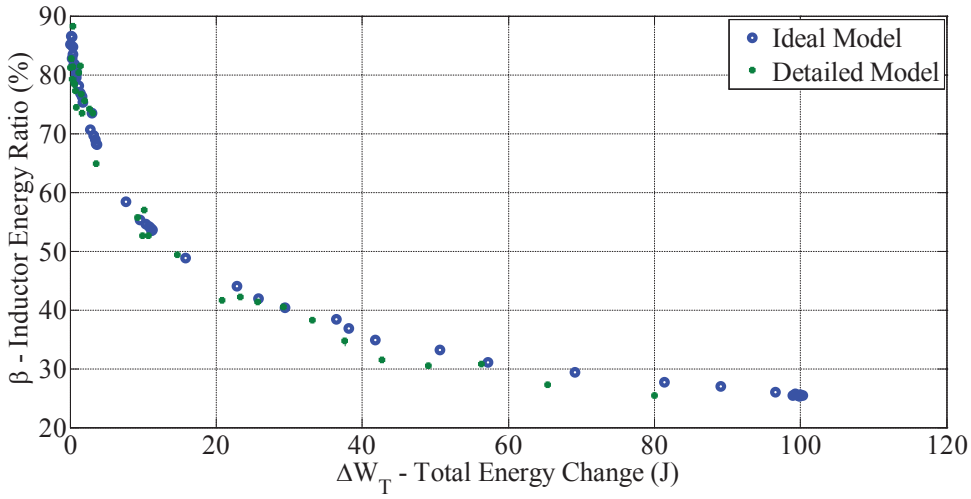

Figure 4-15: Energy Data Sets for both Ideal and Detailed Model

Green dots in the Figure 4-15 represent the data set for the detailed model while the blue dots belong to the ideal model. As it is shown in the figure, the two data sets are relatively close to each other. To get the most accurate data from the simulation, another curve fitted on the new data set and it is shown in Figure 4-16.

The rational function for the fitted curve in Figure 4-16 is

$$\beta = \frac{-0.06935\,\Delta W_T^2 + 22.12\,\Delta W_T + 999.3}{\Delta W_T + 12.03}. \qquad 4.28$$

Equation 4.28 is used to form the close loop controller for the detailed model of boost converter in the simulation.

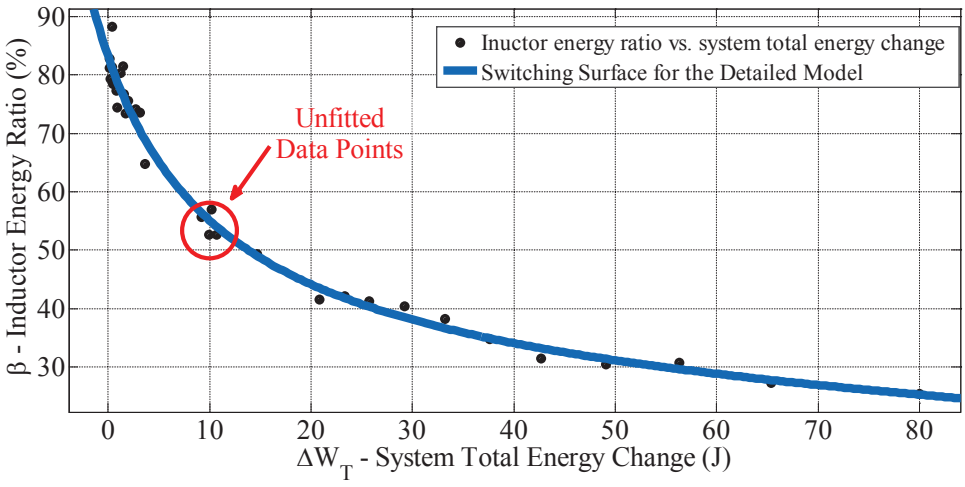

Figure 4-16: Switching Surface for detailed Model of the System

Parameters of the detailed model simulation for the boost converter shown in Figure 3-1 are presented in Table C.

Table C: Detailed Simulation Parameters

Parameter	***Value***
V_{in}	24 V
L	0.1 mH
R_L	1 μΩ
C	1000 μF
ESR	1 μΩ
R	2 Ω
q_1	TK72A08N1
R_{ds}	3.7 mΩ
R_g	10 Ω
C_{gs}	1 nF
q_2	1N4007
$R_{forward}$	1 mΩ
Switching Frequency	10 KHz

4.3.2 Results

The simulation is has been ran for four different scenarios, these scenarios are defined differently to make sure that the closed loop controller has wide range of operation based on the change in total energy stored in the boost converter. Results for these scenarios are presented in the following subsections.

4.3.2.1 Scenario 1

The first set of results is for the scenario with relatively low total energy change of the system. In this scenario duty cycle changed from 0.3 to 0.6 and the total energy stored in the boost converter increased 1.4332 J. Capacitor voltage for the detailed model of the boost converter is shown in Figure 4-17, the boost converter moved to the new operating point with the proposed closed loop bang-bang controller in minimum time. The small oscillation in the capacitor voltage is because of calculation errors in the curve fitting tool.

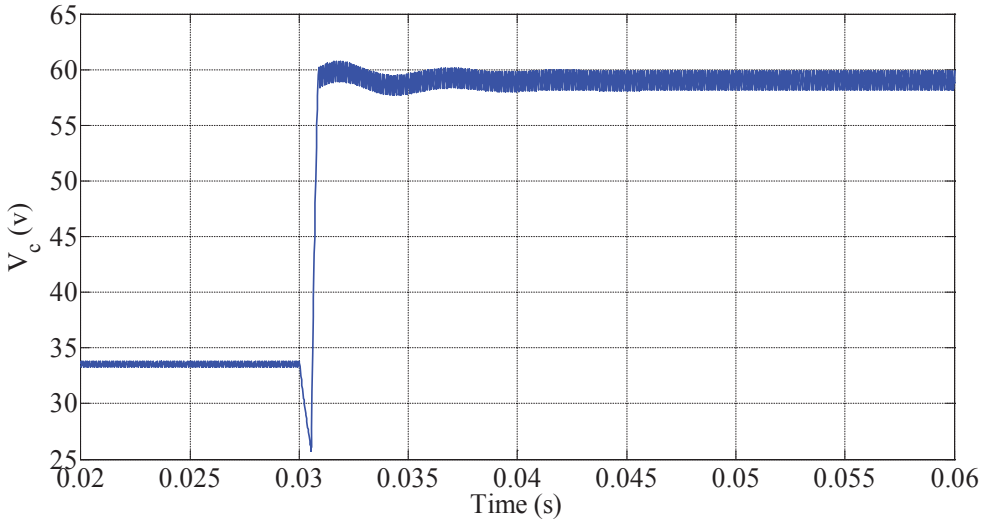

Figure 4-17: Capacitor Voltage for a step change between duty cycle of 0.3 to 0.6 under control of presented controller

Inductor current of the detailed model of the boost converter is presented in Figure 4-18. The small vibration is result of inaccurate t_2 estimation which might be happened because of curve fitting errors.

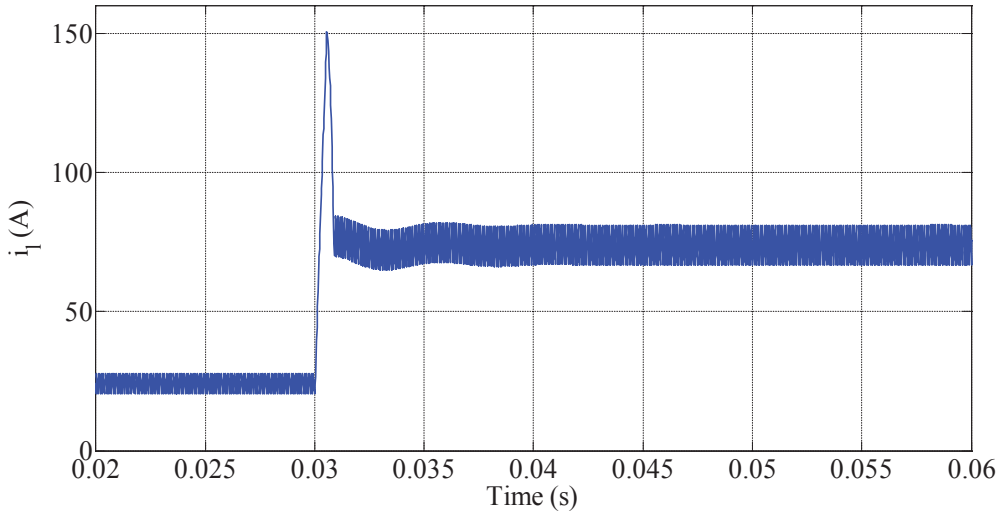

Figure 4-18: Inductor Current for a step change between duty cycle of 0.3 to 0.6 under control of presented controller

4.3.2.2 Scenario 2

This scenario has a medium change in total energy of the system which is 10.7021 J and the duty cycle is changed from 0.1 to 0.8. Oscillations in the capacitor voltage in Figure 4-19 and inductor current are more than the first scenario. From Figure 4-16, it is seen that the curve doesn't fit the data point in the medium range of total energy change in the system (pointed with the red arrow) and it will cause errors in the controller. By increasing the data set it is possible to get more accurate curve and design a better controller.

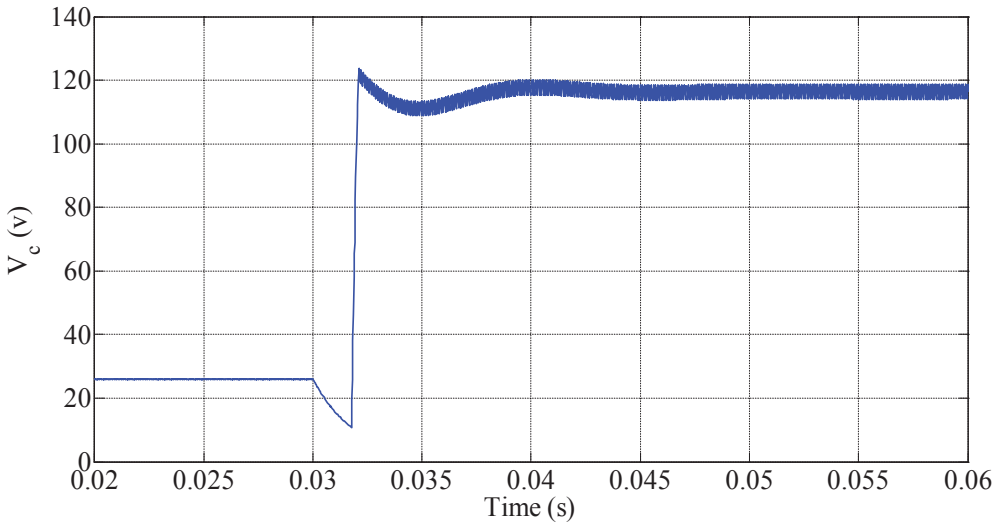

Figure 4-19: Capacitor Voltage for a step change between duty cycle of 0.1 to 0.8 under control of presented controller

Figure 4-20 shows the inductor current for the detailed model of the boost converter. As it is seen in the figure, inductor current passed the desired value at its final operating point and came back to it after the bang-bang control is finished; but the bang-bang control stopped as soon as the capacitor voltage reached its desired value at the final

point. The reason behind this is the algorithm procedures that find the final switching time (t_3) based on capacitor voltage and any error in finding t_2 might cause oscillations in the system's response.

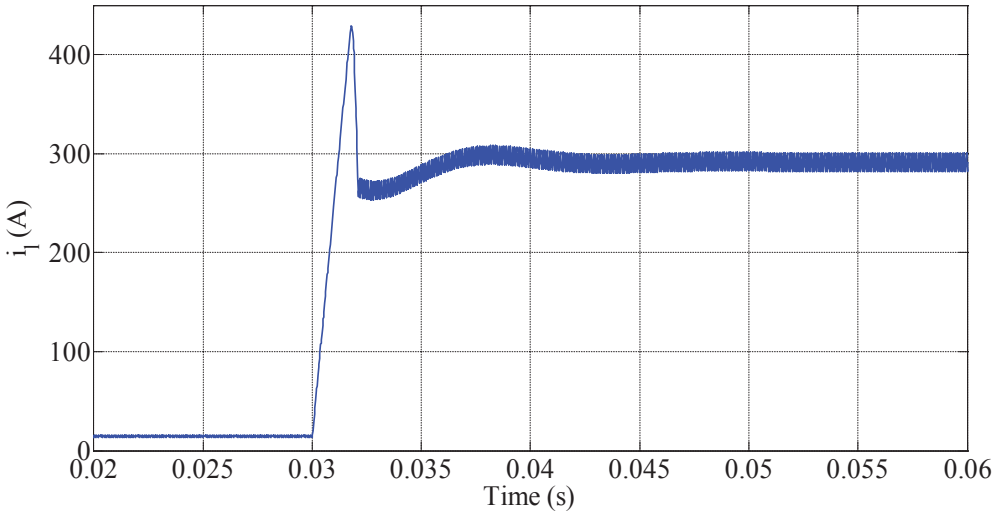

Figure 4-20: Inductor Current for a step change between duty cycle of 0.1 to 0.8 under control of presented controller

4.3.2.3 Scenario 3

Largest change in the total energy which is saved in the system is shown in this scenario. By changing the output voltage from 26 V (duty cycle = 0.1) to 215 V (duty cycle = 0.9), the total energy stored in the boost converter increased 80.0428 J. However this scenario is far away from the reality because of huge inductor current but the designed controller was able to handle it. Figure 4-21 shows the capacitor voltage of the detailed modeled boost converter in this scenario, it is seen that the capacitor voltage reached the desired set point however it didn't happen in minimum time.

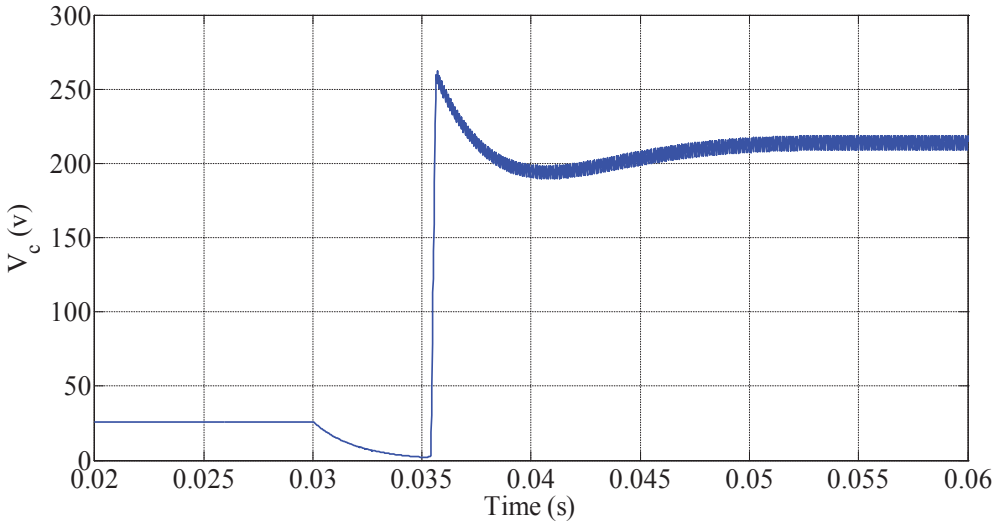

Figure 4-21: Capacitor Voltage for a step change between duty cycle of 0.1 to 0.9 under control of presented controller

The inductor current of the detailed model boost converter is shown in Figure 4-21, reaching the final value in a simulation which is far away from practical circuit shows the robustness of the proposed system in a way that it was able to handle the situation however it didn't happen in the shortest time possible.

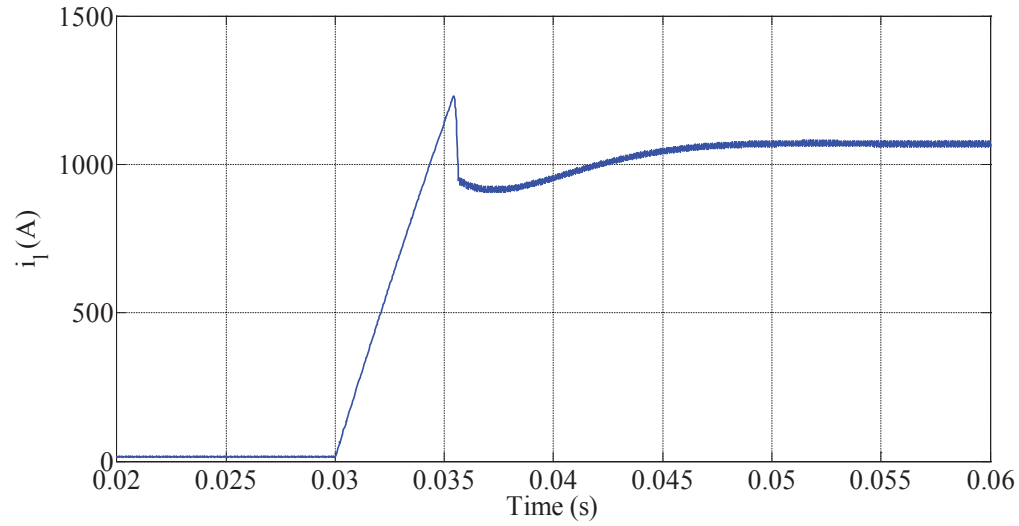

Figure 4-22: Inductor Current for a step change between duty cycle of 0.1 to 0.9 under control of presented controller

4.3.2.4 Scenario 4

Another type of energy change in the system is examined in this scenario. The other reason for changing the total energy of the boost converter is load change, the controller should be able to keep the output voltage in the fixed set point when the load is changed. By changing the load and keeping the output voltage constant, the output current of the boost converter will change. In this scenario, the load is increased and the total energy of the boost converter is also increased as a result. Following figures show the inductor current and capacitor voltage during the load change. The capacitor voltage in this scenario is shown in Figure 4-23, the voltage remains at its previous value after a fast transient to compensate the energy change of the system.

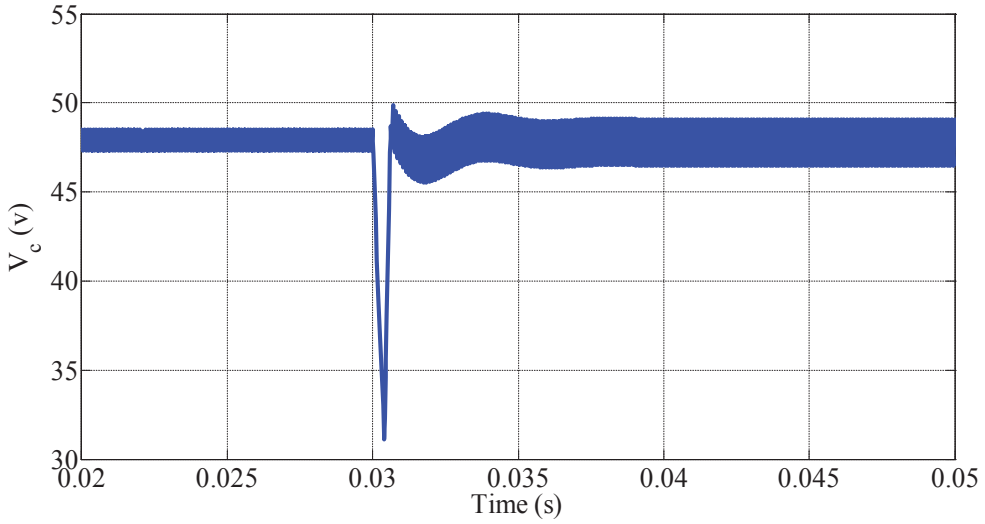

Figure 4-23: Capacitor Voltage of the detailed model of the boost converter during the step load change with the proposed minimum-time optimal controller

The inductor current of the detailed model during the step load change is shown in Figure 4-24. It is seen that the inductor current is changed after the step load change to compensate the energy change in the system in the minimum-time.

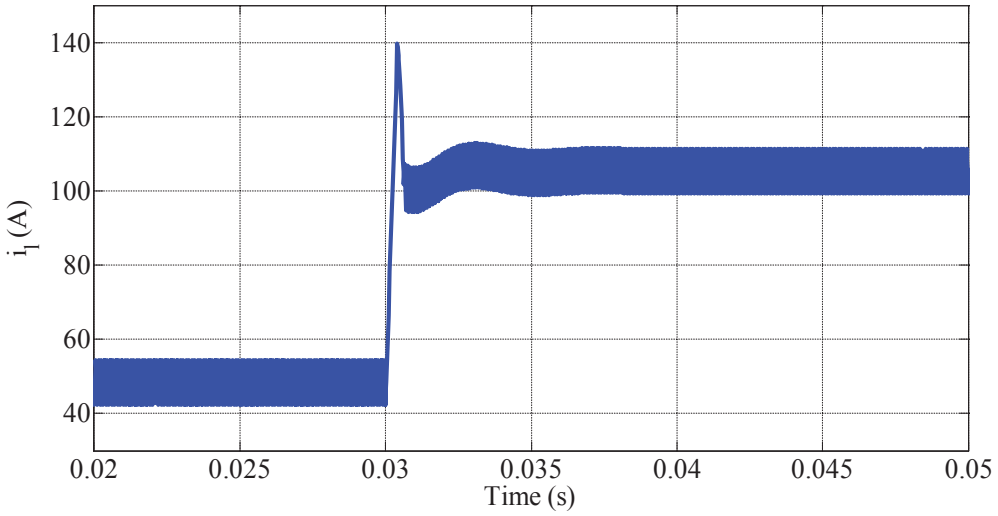

Figure 4-24: Inductor Current of the detailed model of the boost converter during the step load change with the proposed minimum-time optimal controller

The controller needs to be changed a slightly to handle this scenario. In the previous scenarios, the final switching time was obtained from comparing the output voltage with the new desired set point. In this scenario the output voltage has the same set point before and after the load change, as a result it cannot be used to generate the final switching signal. As an alternative, the final switching signal is generated by comparing the inductor current with its desired value after the load change.

4.3.3 Discussion

The controller design in this study started with simulating a dc-dc boost converter through its differential equations in MATLAB. To simplify the modeling an equations, it is assumed that all elements of the converter are ideal. The time optimal solution for the boost converter moving between two states is presented and solved in average mode first, and then it is expanded to the switched mode boost converter.

Two topologies of the boost converter circuit are presented based on the position of the switch and stability of each topology is investigated. The energy flow in each topology discussed and an energy based control method developed for the ideally modeled dc-dc boost converter. Then, the energy based solution expanded to the detailed model of the boost converter and the differences of the switching surface between the ideal model and the detailed model explored.

A comparison between data points for the ideal model and the detailed model has been done. The presented data points for the ideal model and the detailed model are fairly on top of each other when the total energy change in the system is less than 5 J. The

calculated rational function for the ideal model can be used for detail model as well, if the system is about to run for the total energy change less than 5 J. However the switching surface for the detailed model and the ideal model are fairly close in this range, but there might be some oscillations in the system if the ideal switching surface be used for the real system.

At the end, four different scenario of energy change in the system is defined and the detailed model of the boost converter simulated in the scenarios. Three of the scenarios were based on changing the output voltage set point with different amount of energy change in the system while the last scenario was exploring the load change in the system. The designed controller was able to handle all the scenarios and provided the near time-optimal transition between the different states of the boost converter.

Chapter 5: Conclusion and Future Works

5.1 Conclusion

A time optimal control method, based on the total energy of the system and its changes is presented and developed for a dc-dc boost converter. Different methods such as developing switching surface based on the capacitor current estimation and finding the time optimal switching time from capacitor charge balance principle were applied to buck converter before, but it is not possible to apply any of them to the boost converter. The reason that it is not possible to apply aforementioned methods to boost converters is the boost converter topology during the switching period. In one part of the switching (when the switch is on), the dynamic elements of the circuit (inductor and capacitor) are completely separated from each other. As a result, the capacitor current or the capacitor state of charge cannot be related to state of the inductor. Total energy of the system is a mutual parameter between the two topologies of the boost converter; on the other hand, it is easier to monitor the energy of the capacitor in comparison with measuring its current. Because of the aforementioned reasons, the presented time optimal method formed on the basis of the total energy of the system. The presented method uses a predefined switching surface which decreasing the time and amount of the calculations for the controller. As it is shown in the result section, the energy based time optimal

controller was able to move the dc-dc boost converter from an initial state to a desired final state in optimum time for different scenarios.

5.2 Future Works

This study can be expanded in different ways; first of all, some interfaces are needed to be designed and fabricated to implement the method on the real boost converter circuits. As it is shown in the results, the controller should generate the switching signals in less than a micro second accuracy. The only devices which are able to do this fast switching rule are analog circuits and FPGAs. Analog circuits might be even faster than FPGAs but the problem of using them is that it is not possible to change the design after they are made, so a new analog circuit should be designed for each revision or correction which is very time consuming. The other down side of the analog circuits is that each controller circuit can be used for just one scenario, because the analog circuits cannot save the switching surface to apply the control method in different conditions. Besides having a fast controller circuit, very fast sensors and ADC modules are also needed to gather enough data during the switching period for the FPGA to generate the switching signals.

As it is shown in the results, the most important part of the algorithm for achieving the minimum time transition with the least vibration is the switching surface. Adding a learning algorithm to the method to increase the accuracy of the surface can increase the robustness of the system. The learning algorithm can be used in both designing and implementing the method, first the learning algorithm can be used to form the initial

switching surface and in the second stage it can be used during the working period of the controller to improve the switching surface based on the occurred scenarios which might not be considered while the switching surface formed.

References

[1] M. Aten, G. Towers, C. Whitley, P. Wheeler, J. Clare and K. Bradley, "Reliability comparison of matrix and other converter topologies.," *IEEE Transactions on Aerospace and Electronic Systems*, vol. 42, no. 3, pp. 867-875, 2006.

[2] A. Capel and D. O'Sullivan, "Very high frequency regulator for space applications.," in *IEEE Power Electronics Specialists Conference*, 1996, pp. 846-852.

[3] L. Guao, J.Y. Hung and R.M. Nelms, "PID controller modifications to improve steady-state performance of digital controllers for buck and boost converters.," in *IEEE Applied Power Electronics Conference and Exposition*, 2002, pp. 381-388.

[4] H. Hu, V. Yousefzadeh and D. Maksimovic, "Nonlinear control for improved dynamic response of digitally controlled dc-dc converters.," in *IEEE Power Electronics Specialists Conference*, 2006, pp. 1-7.

[5] D. Biel, L Martinez, J. Tenor, B. Jammes and J.C. Marpinard, "Optimum dynamic performance of a buck converter.," in *IEEE International Symposium on Circuits and Systems*, 1996, pp. 589-592.

[6] N.C. Singer and W.P. Seering, "Preshaping Command inputs to Reduce System Vibration," *Journal of Dynamic Systems, Measurement, and Control*, pp. 76 - 82,

1990.

[7] N. Singer, W. Singhose and E. Kriikku, "An input shaping controller enabling cranes to move without sway.," in *ANS 7th topical meeting on robotics and remote systems*, 1997.

[8] W. Singhose, D. Kim and M. Kenison, "Input shaping control of double-pendulum bridge crane oscillations.," *Journal of Dynamic Systems, Measurement, and Control*, vol. 130, no. 3, May 2008.

[9] W.E. Singhose, A.K. Banerjee and W.P. Seering, "Slewing flexible spacecraft with deflection-limiting input shaping.," *Journal of Guidance, Control, and Dynamics.*, vol. 20, no. 2, pp. 291-298, 1997.

[10] W.E. Singhose and N.C. Singer, "Effects of Input Shaping on Two-Dimensional Trajectory Following," *IEEE Transactions on Robotics and Automation*, vol. 12, no. 6, pp. 881-887, 1996.

[11] W. Singhose and N. Singer, "Initial investigations into the effects of input shaping on trajectory following.," in *IEEE Proc. of American Control Conference*, 1994, pp. 2526-2532.

[12] W.P. Seering, N. C. Singer and W.E. Singhose, "Input Shaping for Vibration Reduction with Specified Insensitivity to Modeling Errors," in *Japan-USA Sym. on Flexible Automation*, 1996, pp. 307 - 313.

[13] W.P. Seering and N.C. Singer W.E. Singhose, "Input shaping for vibration reduction with specified insensitivity to modeling errors.," in *Japan-USA Sym. on Flexible Automation*, 1996, pp. 307-313.

[14] W.E. Singhose, W.P. Seering and N.C. Singer, "Shaping inputs to reduce vibration: a vector diagram approach.," in *International Conference on Proc. in Robotics and Automation*, 1990, pp. 922-927.

[15] L.Y. Pao, "Multi-input shaping design for vibration reduction," *Automatica 35*, vol. 1, pp. 81-89, 1999.

[16] W.P. Seering and T.D. Tuttle, "A zero-placement technique for designing shaped inputs to suppress multiple-mode vibration," in *Proc. of American Control Conf.*, Baltimore, 1994, pp. 2523 - 2537.

[17] W. Singhose and T. Singh, "Tutorial on input shaping/time delay control of maneuvering flexible structures," in *Proce. of American Control Conf.*, Anchorage, 2002, pp. 1717 - 1729.

[18] W. E. Singhose and L.Y. Pao, "On the equivalence of minimum time input shaping with traditional time-optimal control," in *Proc. of 4th IEEE Conf. on Control Applications*, Albany, 1995, pp. 1120 - 1125.

[19] A.E. Bryson and Y.-C. Ho, *Applied Optimal Control: Optimization, Estimation, And Control*. Washington D.C., USA: John Wiley & Sons, 1975.

[20] J. Wing and C.A. Desoer, "The multiple-input minimal time regulator problem (general theory).," *IEEE Transaction on Automatic Control*, vol. 8, no. 2, pp. 125-136, 1963.

[21] A.S.I. Zinober and A.T. Fuller, "The sensitivity of nominally time-time optimal control systems to parameter variation," *International Journal of Control*, vol. 17, no. 4, pp. 673-703, 1973.

[22] G.E. Pitel and P.T. Krein, "Minimum-time digital control with raster surfaces.," in *IEEE Workshop on Control and Modeling for Power Electronics*, 2008, pp. 1-8.

[23] T.D. Tuttle and W.P. Seering, "Creating Time-Optimal Commands with Practical Constraints," *Journal of Guidance, Control and Dynamic*, vol. 22, no. 2, pp. 241-250, March-April 1999.

[24] C.Y. Kaya and S.K. Lucas S.T. Simakov, "Computations for time-optimal bang–bang control using a Lagrangian formulation.," in *Triennial World Congress*, Barcelona, 2002.

[25] S.B. Andersson and Z. Shen, "Minimum time control of a second-order system," in *49th IEEE Conference on Decision and Control*, 2010, pp. 4819 - 4824.

[26] N. Sadegh and B. Driessen, "Minimum time trajectory optimization and learning," *Journal of dynamic systems, measurement, and control*, vol. 121, no. 2, pp. 213 - 217, 1999.

[27] S. Gomáriz, E. Alarcon, J.A. Martínez, A. Poveda, J. Madrenas and F. Guinjoan, "Minimum time control of a buck converter by means of fuzzy logic approximation.," in *IEEE Proc. of Annual Conference of Industrial Electronics Society*, 1998, pp. 1060-1065.

[28] R. Miftakhutdinov, "Optimal design of interleaved synchronous buck converter at high slew-rate load current transients.," in *IEEE annual Power Electronics Specialists Conference*, 2001, pp. 1714-1718.

[29] T. Hamada, T. Nabeshima, T. Sato and T. Nakano S. Kanemaru, "Analysis and optimum design of a buck-type dc-to-dc converter employing load current feedforward.," in *IEEE Annual Power Electronics Specialists Conference*, 1998, pp. 309-314.

[30] S.M.R. Rafiei, A. Amirahmadi, and G. Griva, "Chaos rejection and optimal dynamic response for boost converter using SPEA multi-objective optimization approach," in *35th Annual Conference of IEEE Industrial Electronics*, 2009, pp. 3315 - 3322.

[31] L.Y. Pao and G. F. Franklin, "Proximate time-optimal control of third-order servomechanisms," *IEEE Transaction on Automatic Control*, vol. 38, no. 4, pp. 560-580, 1993.

[32] L.Y. Pao and G.F. Franklin, "The robustness of a proximate time-optional controller [optional read optimal].," *IEEE Transactions on Automatic Control*, vol.

39, no. 9, pp. 1963-1966, 1994.

[33] V. Yousefzadeh, A. Babazadeh, B. Ramachandran, L.Y. Pao, D. Maksimovic, and E. Alarcon, "Proximate time optimal digital control for DC-DC converters," in *IEEE Power Electronics Specialists Conf.*, 2007, pp. 124 - 130.

[34] G. Feng, E. Meyer and Y.F. Liu, "High performance digital control algorithms for DC-DC converters based on the principle of capacitor charge balance," in *37th IEEE Power Electronics Specialists Conf.*, 2006, pp. 1 - 7.

[35] G. Feng, E. Meyer, and Y.F. Liu, "A new digital control algorithm to achieve optimal dynamic performance in DC-to-DC converters," *IEEE Transactions on Power Electronics*, vol. 22, no. 4, pp. 1489 - 1498, 2007.

[36] E.Meyer, G.Feng and Y.F. Liu, "Novel digital controller improves dynamic response and simplifies design process of voltage regulator module," in *Twenty Second Annual IEEE Applied Power Electronics Conf.*, 2007, pp. 1447 - 1453.

[37] H. Sira-Ramírez and R. Silva-Ortigoza, *Control design techniques in power electronic devices*. Germany: Springer Science & Business Media, 2006.

[38] E. Hendricks, O. Jannerup and P.H. Sørensen, *Linear Systems Control: deterministic and stochastic methods.* Berlin: Springer Science & Business Media, 2008.

[39] JJ.E. Slotine and W. Li, *Applied nonlinear control*. Englewood Cliffs, NJ: Prentice-

Hall, 1991.

[40] S. Boyd and C. Barratt, *Linear Controller Design: Limits of Performance*.: Prentice-Hall, 1991.

[41] A.P. Sage and C.C. White, *Optimum systems control*, 2nd ed. Englewood Cliffs, New Jersey: Prentice-Hall, 1977.

[42] P. Gupta and A. Patra, "A Stable Energy-Based Control Strategy for DC-DC Boost Converter Circuit.," in *IEEE Power Electronics Specialists Conference*, Aachen, 2004, pp. 3642-3646.

[43] P. Gupta and A. Patra, "Super-stable energy based switching control scheme for DC-DC buck converter circuits.," in *IEEE International Symposium on Circuits and Systems*, 2005, pp. 3063-3066.

[44] N. Mohan, T.M. Undeland and W.P. Robbins, *Power Electrinics: Converter, Applications, and Design.*: Joun Wiley & Sons, 2003.

Appendix A: Data points gathered from running different scenarios

Table A-1: Data from detailed model

D1	D2	dt1	dt2	Ui1	Ui2	Ui3	Uc1	Uc2	Uc3	dUi1	dUc1	dUi2	dUc2	DU	%
0.1	0.2	0.00082	0.00033	0.008745	0.0541	0.0173	0.3385	0.3119	0.4288	-0.04535	0.0266	0.0368	-0.1169	-0.09885	81.13841
0.2	0.3	0.00013	0.000285	0.0126	0.1106	0.0295	0.4327	0.38	0.5664	-0.098	0.0527	0.0811	-0.1864	-0.1506	82.7551
0.4	0.5	0.000275	0.000245	0.039	0.4378	0.1132	0.785	0.5962	1.1173	-0.3988	0.1888	0.3246	-0.5211	-0.4065	81.39418
0.5	0.6	0.0004	0.00023	0.085	0.9309	0.2773	1.1407	0.7646	1.7051	-0.8459	0.3761	0.6536	-0.9405	-0.7567	77.26682
0.6	0.7	0.00067	0.000245	0.2225	2.5381	0.789	1.794	0.9179	3.1822	-2.3156	0.8761	1.7491	-2.2643	-1.9547	75.5355
0.1	0.3	0.000151	0.00037	0.008746	0.1219	0.0322	0.3385	0.2911	0.5614	-0.11315	0.0474	0.0897	-0.2703	-0.24635	79.27215
0.2	0.4	0.000228	0.00037	0.0126	0.2479	0.0403	0.4327	0.3445	0.7891	-0.2353	0.0882	0.2076	-0.4446	-0.3841	88.22779
0.3	0.5	0.000329	0.000308	0.0208	0.4892	0.1219	0.571	0.4109	1.0976	-0.4684	0.1601	0.3673	-0.6867	-0.6277	78.41588
0.4	0.6	0.0005	0.000314	0.039	1.0799	0.2438	0.785	0.4761	1.7835	-1.0409	0.3089	0.8361	-1.3074	-1.2033	80.32472
0.5	0.7	0.0008	0.0003	0.085	2.6632	0.7505	1.1408	0.5126	3.1725	-2.5782	0.6282	1.9127	-2.6599	-2.6972	74.18742
0.6	0.8	0.00157	0.000262	0.2225	9.4393	4.3043	1.7942	0.3735	6.9249	-9.2168	1.4207	5.135	-6.5514	-9.2125	55.71348
0.1	0.4	0.000239	0.000385	0.008746	0.2476	0.0602	0.3386	0.2666	0.7609	-0.23885	0.072	0.1874	-0.4943	-0.47375	78.45784
0.3	0.6	0.00054	0.00035	0.0208	1.1095	0.2231	0.571	0.3327	1.8019	-1.0887	0.2383	0.8864	-1.4692	-1.4332	81.41821
0.4	0.7	0.00087	0.00031	0.039	2.7411	0.7551	0.7849	0.3289	3.2054	-2.7021	0.456	1.986	-2.8765	-3.1366	73.49839
0.5	0.8	0.00167	0.00027	0.0851	9.3754	4.4841	1.1408	0.2148	6.67	-9.2903	0.926	4.8913	-6.4552	-9.9282	52.64954
0.1	0.5	0.00037	0.000376	0.008746	0.517	0.1388	0.3386	0.2338	1.0943	-0.50825	0.1048	0.3782	-0.8605	-0.88575	74.41155
0.2	0.6	0.000558	0.000368	0.0127	1.1076	0.2675	0.4328	0.2477	1.7529	-1.0949	0.1851	0.8401	-1.5052	-1.5749	76.72847
0.4	0.8	0.00171	0.000295	0.039	9.2341	3.9932	0.785	0.142	7.0131	-9.1951	0.643	5.2409	-6.8711	-10.1823	56.99666
0.1	0.6	0.000568	0.000375	0.008745	1.1097	0.3011	0.3386	0.1919	1.722	-1.10096	0.1467	0.8086	-1.5301	-1.67576	73.44533
0.1	0.7	0.000924	0.000342	0.008746	2.7243	0.964	0.3386	0.1344	2.9782	-2.71555	0.2042	1.7603	-2.8438	-3.59485	64.82286
0.1	0.8	0.00177	0.000295	0.008746	9.2791	4.401	0.3386	0.0577	6.6484	-9.27035	0.2809	4.8781	-6.5907	-10.7021	52.62043
0.1	0.9	0.00547	0.000186	0.008746	77.3069	57.647	0.3386	0.002863	22.7431	-77.2982	0.335737	19.6599	-22.7402	-80.0428	25.43385
0.5	0.825	0.00208	0.000256	0.0851	13.8946	7.081	1.1408	0.1426	8.8002	-13.8095	0.9982	6.8136	-8.6576	-14.6553	49.33995
0.5	0.85	0.0027	0.000245	0.0851	22.294	12.9294	1.1408	0.0767	11.6412	-22.2089	1.0641	9.3646	-11.5645	-23.3447	42.16598
0.7	0.85	0.00235	0.00022	0.7543	22.1295	13.242	3.1941	0.3052	11.571	-21.3752	2.8889	8.8875	-11.2658	-20.8646	41.57856
0.7	0.87	0.0031	0.00022	0.7543	34.6222	21.6729	3.1941	0.1442	15.4902	-33.8679	3.0499	12.9493	-15.346	-33.2147	38.23473
0.7	0.86	0.00268	0.000225	0.7543	27.3074	16.3449	3.1941	0.2195	13.3386	-26.5531	2.9746	10.9625	-13.1191	-25.7351	41.2852
0.7	0.865	0.00288	0.000225	0.7543	30.6912	18.5799	3.1941	0.1797	14.5617	-29.9369	3.0144	12.1113	-14.382	-29.1932	40.45609
0.7	0.875	0.00333	0.00021	0.7543	38.9593	25.6959	3.1941	0.1145	15.8893	-38.205	3.0796	13.2634	-15.7748	-37.6368	34.7164
0.7	0.88	0.00358	0.0002	0.7543	43.9312	30.3667	3.1941	0.0892	16.2524	-43.1769	3.1049	13.5645	-16.1632	-42.6707	31.4161
0.7	0.885	0.00388	0.000198	0.7543	50.2375	35.1607	3.1941	0.0662	17.8586	-49.4832	3.1279	15.0768	-17.7924	-49.0709	30.46852
0.7	0.89	0.0042	0.000198	0.7543	57.3803	39.9865	3.1941	0.048	20.2988	-56.626	3.1461	17.3938	-20.2508	-56.3369	30.71699
0.7	0.895	0.00458	0.000188	0.7543	66.3655	48.5037	3.1941	0.0328	20.8323	-65.6112	3.1613	17.8618	-20.7995	-65.3876	27.22371

Table A-2: Data from ideal model

D1	D2	t1	t2	dUi1	dUc1	dUi2	dUc2	DU	%
0.1	0.2	1.000777	1.0004099	-0.0437	0.0261	0.0372	-0.1204	-0.1008	85.12586
0.2	0.3	1.000117125	1.0004	-0.0922	0.0497	0.0798	-0.1872	-0.1499	86.55098
0.3	0.4			-0.1854	0.0925	0.1602	-0.3048	-0.2375	86.40777
0.4	0.5	1.000251282	1.000496	-0.3829	0.1778	0.3243	-0.5297	-0.4105	84.69574
0.5	0.6			-0.865	0.367	0.69805	-1.016	-0.81595	80.69942
0.6	0.7	1.0006325	1.000866	-2.2918	0.8444	1.6847	-2.2415	-2.0042	73.5099
0.7	0.8	1.001268	1.00495	-8.689	2.3002	5.0695	-6.2913	-7.6106	58.34388
0.8	0.9	1.004552	1.004732	-92.45	7.1357	24.9073	-28.725	-89.132	26.94137
0.1	0.3	1.000144	1.0005257	-0.1111	0.0477	0.092	-0.2794	-0.2508	82.80828
0.2	0.4	1.0002138	1.0005556	-0.2279	0.0866	0.1903	-0.4363	-0.3873	83.50154
0.3	0.5			-0.4693	0.1584	0.384	-0.7236	-0.6505	81.82399
0.4	0.6	1.0004746	1.000776	-1.0285	0.3023	0.8033	-1.3013	-1.2242	78.10404
0.5	0.7	1.000777	1.0010639	-2.6338	0.6224	1.8632	-2.6747	-2.8229	70.74189
0.6	0.8	1.0015273	1.0017883	-9.4672	1.4098	5.231	-6.7934	-9.6198	55.25393
0.7	0.9	1.00524	1.005425	-95.8463	3.1876	24.8651	-28.837	-96.6306	25.94268
0.1	0.4	1.00023299	1.0006315	-0.2388	0.0739	0.1948	-0.5165	-0.4866	81.57454
0.2	0.5	1.0003445	1.000708	-0.4969	0.1311	0.3981	-0.8323	-0.8	80.11672
0.3	0.6	1.00052	1.00086	-1.0845	0.2383	0.843	-1.4529	-1.4561	77.73167
0.4	0.7	1.000845	1.001161	-2.7318	0.4564	1.9038	-2.8653	-3.2369	69.69031
0.5	0.8	1.00164	1.0019175	-9.63352	0.9287	5.2523	-6.9771	-10.4296	54.52109
0.6	0.9	1.0055	1.005686	-97.0293	1.7945	24.8868	-28.9112	-99.2592	25.64875
0.1	0.5	1.00036	1.000759	-0.5016	0.1076	0.399	-0.9044	-0.8994	79.54545
0.2	0.6	1.000544	1.000911	-1.0971	0.1888	0.8371	-1.541	-1.6122	76.30116
0.3	0.7	1.000882	1.001216	-2.7589	0.3445	1.901	-2.9624	-3.4758	68.90427
0.4	0.8	1.0017	1.001987	-9.6821	0.654	5.2398	-7.0635	-10.8518	54.11842
0.5	0.9	1.005599	1.005785	-96.7346	1.1486	24.5777	-28.6206	-99.6289	25.40735
0.1	0.6	1.0005585	1.0009435	-1.0975	0.1522	0.8268	-1.5962	-1.7147	75.33485
0.2	0.7	1.000904	1.00125	-2.7601	0.2683	1.8819	-3.0146	-3.6245	68.18231
0.3	0.8	1.001733	1.002026	-9.6682	0.484	5.2023	-7.0895	-11.0714	53.80836
0.4	0.9	1.005658	1.005845	-96.72	0.7976	24.7044	-28.7355	-99.9535	25.54218
0.1	0.7	1.000917	1.001274	-2.7488	0.2134	1.873	-3.0596	-3.722	68.13882
0.2	0.8	1.001755	1.002052	-9.6606	0.3717	5.1677	-7.1021	-11.2233	53.49254
0.3	0.9	1.005658	1.005845	-95.5228	0.586	24.2964	-28.3464	-98.9868	25.43518
0.1	0.8	1.00177	1.002071	-9.6538	0.2953	5.1712	-7.141	-11.3283	53.56647
0.2	0.9	1.005717	1.005904	-96.7028	0.4489	24.5606	-28.631	-100.324	25.39802
0.1	0.9	1.005717	1.005904	-96.1725	0.3536	24.3725	-28.4415	-99.8879	25.34248
0.5	0.825	1.002017	1.002335	-14.7253	1.0072	7.1863	-9.2801	-15.8119	48.8024
0.5	0.85	1.00271	1.002956	-24.2731	1.076	10.1771	-12.7418	-25.7618	41.92748
0.7	0.85	1.002355	1.002585	-23.5102	2.8986	10.3495	-12.6163	-22.8784	44.02132
0.7	0.87	1.003136	1.003353	-38.3604	3.0641	14.1073	-16.9525	-38.1415	36.77569
0.7	0.86	1.00271	1.002934	-29.8248	2.9898	12.0194	-14.5642	-29.3798	40.30002
0.7	0.865	1.00291	1.00313	-33.7021	3.0287	12.9194	-18.6637	-36.4177	38.33411
0.7	0.875	1.00339	1.003605	-44.9473	3.0956	15.6573	-15.6097	-41.8041	34.8348
0.7	0.88	1.00367	1.003878	-50.5366	3.1221	16.7445	-21.5744	-52.2444	33.13341
0.7	0.885	1.00399	1.004192	-58.6202	3.1447	18.2133	-19.924	-57.1862	31.07001
0.7	0.89	1.00436	1.004557	-68.7022	3.1632	20.211	-23.7679	-69.0959	29.41827
0.7	0.895	1.00477	1.004961	-80.7952	3.177	22.3153	-26.0735	-81.3764	27.61959

Appendix B: MATLAB code and Simulink Block diagram of ideal model

MATLAB code:

```
clear all;
clc;

Vin=24;
R=2;
fsw=5000;

L=0.0001;
C=0.001;

D1=0.5;
D2=0.6;

il1=48;
vc1=Vin/(1-D1);

il2=75;
vc2=Vin/(1-D2);

U1=0.5*(L*il1*il1+C*vc1*vc1);
U2=0.5*(L*il2*il2+C*vc2*vc2);

dUi=0.5*(L*il2*il2-L*il1*il1);
dU=U2-U1;
comp=dU+0.5*(L*il1*il1);

X=((-0.1008*dU^2+30.32*dU+706.2)/(dU+8.226))/100;

comp1=dUi/(1-X)+0.5*(L*il1*il1);
```

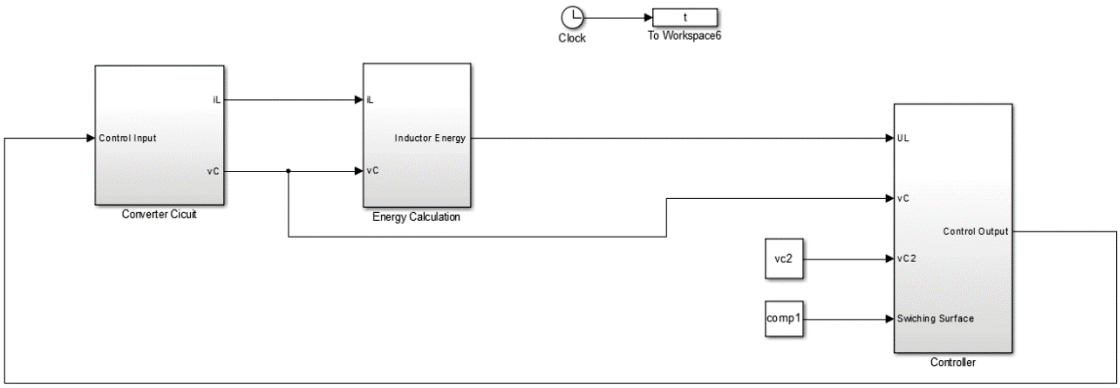

Figure B-1: Simulink Block Diagram for an Ideal Model of the Boost Converter

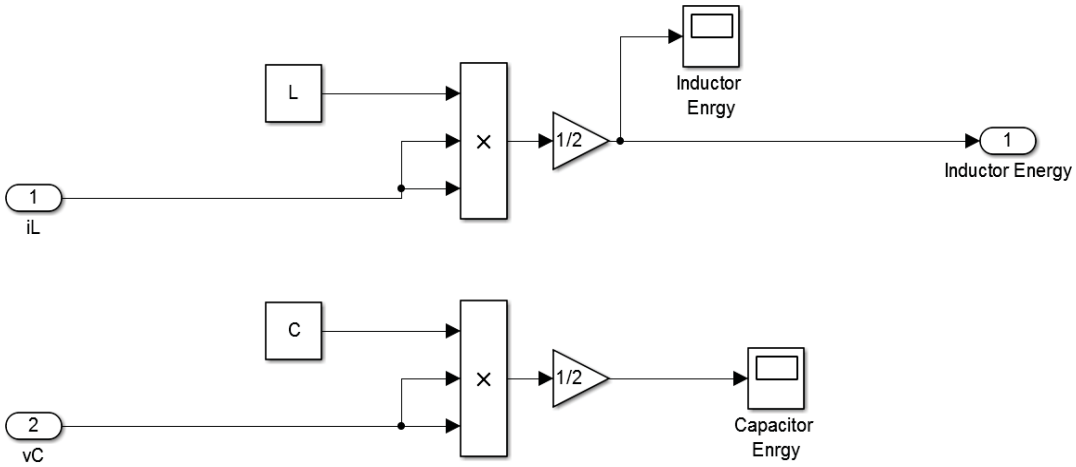

Figure B-2: Energy Calculation Block for Ideal Model of the Boost Converter

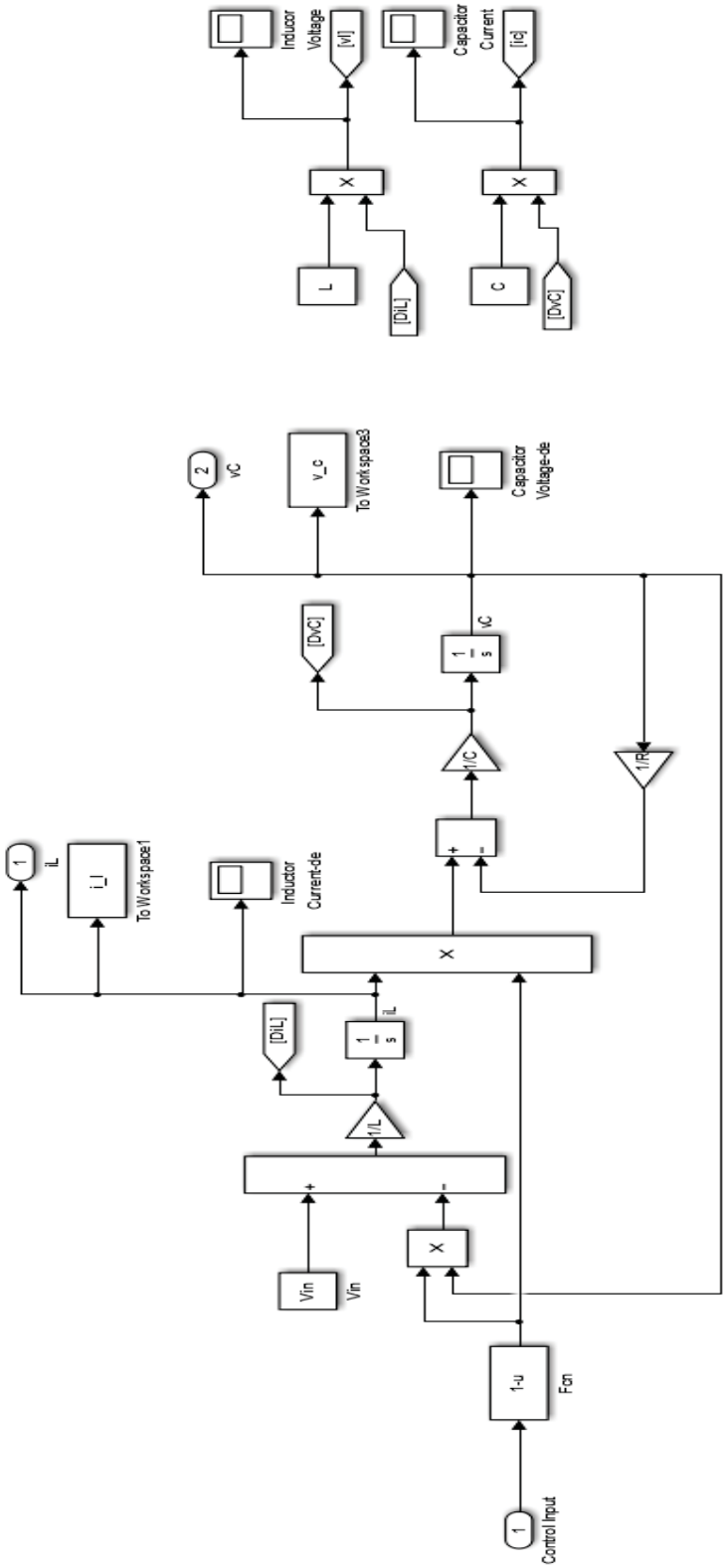

Figure B-3: Ideal Converter Model

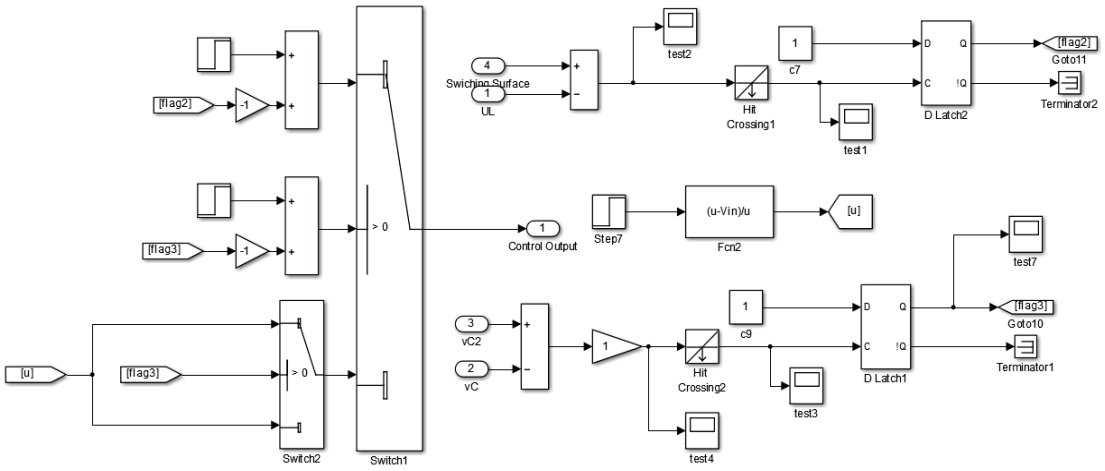

Figure B-4: Controller Block Diagram

Appendix C: MATLAB code and Simulink Block diagram of detailed model

MATLAB Code:

```
clear all;
clc;


Vin=24;
R=2;
fsw=5000;

L=0.0001;
C=0.001;

D1=0.1;
D2=0.8;

il1=14.5;
vc1=Vin/(1-D1);

il2=292;
vc2=Vin/(1-D2);

U1=0.5*(L*il1*il1+C*vc1*vc1);
U2=0.5*(L*il2*il2+C*vc2*vc2);

dUi=0.5*(L*il2*il2-L*il1*il1);
dU=U2-U1;
comp=dU+0.5*(L*il1*il1);

X=((-0.06935*dU^2+22.12*dU+999.3)/(dU+12.03))/100;

comp1=dUi/(1-X)+0.5*(L*il1*il1);
```

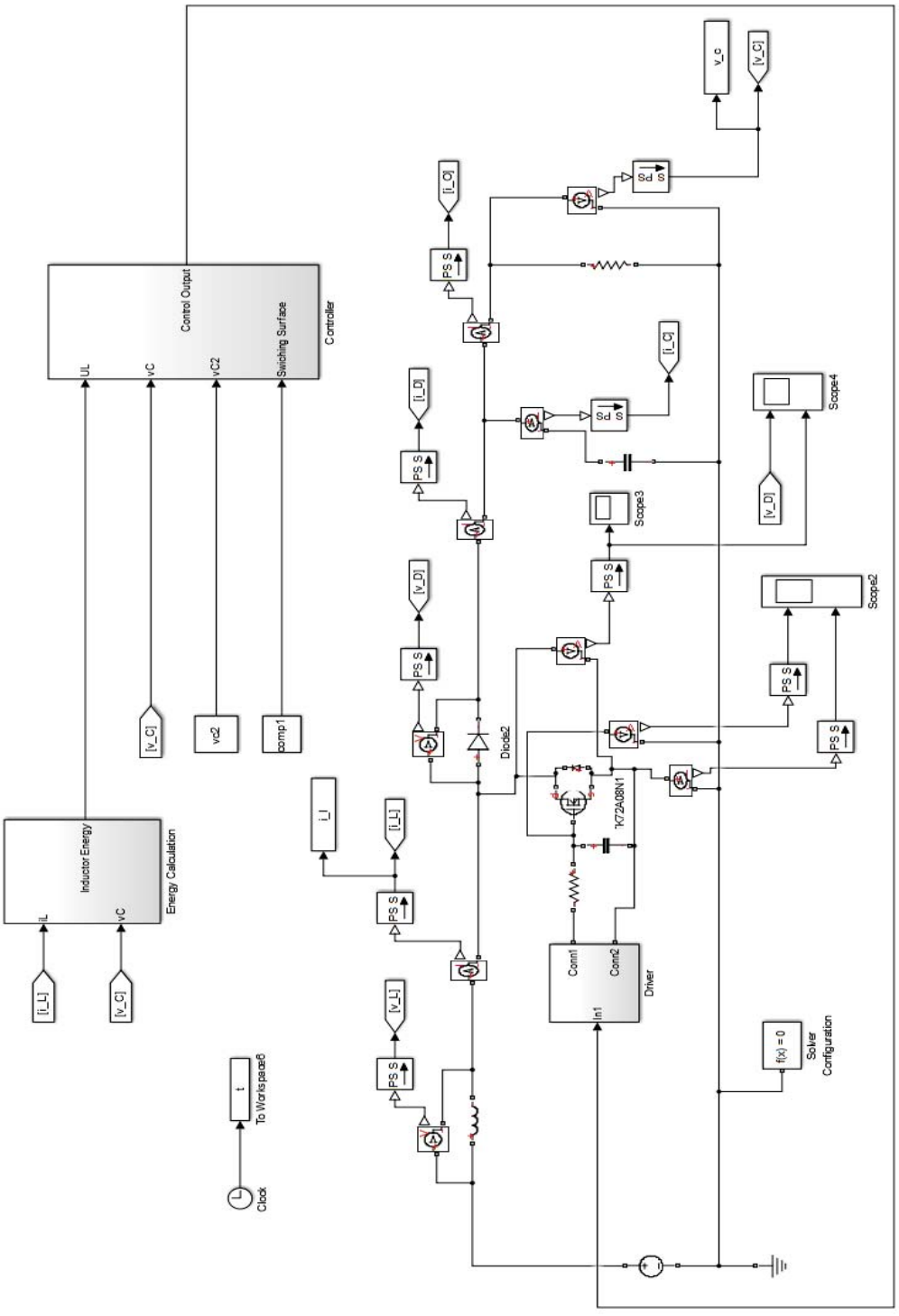

Figure C-1: Boost converter simulation implemented by SimScape toolbox

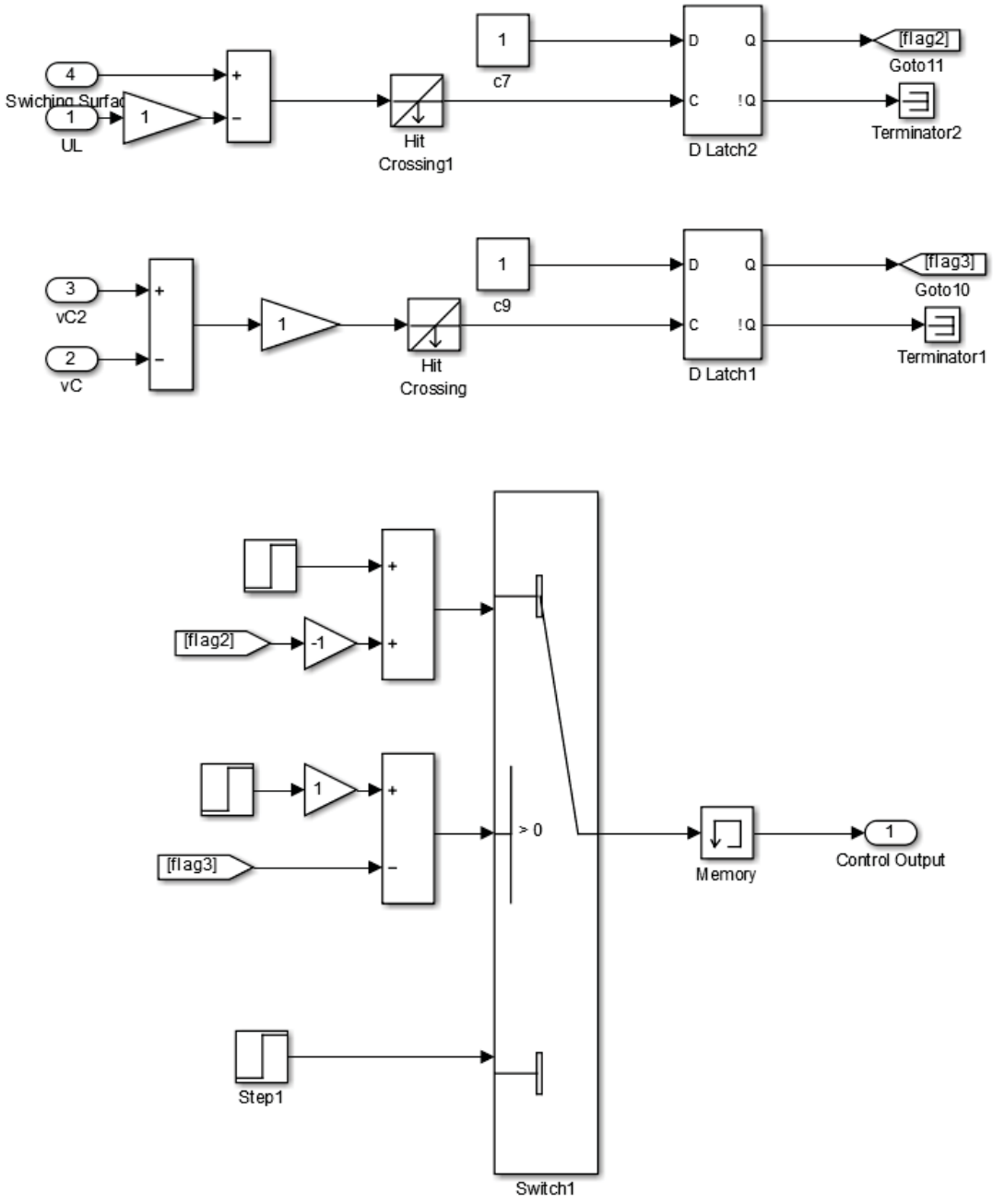

Figure C-2: Controller Block

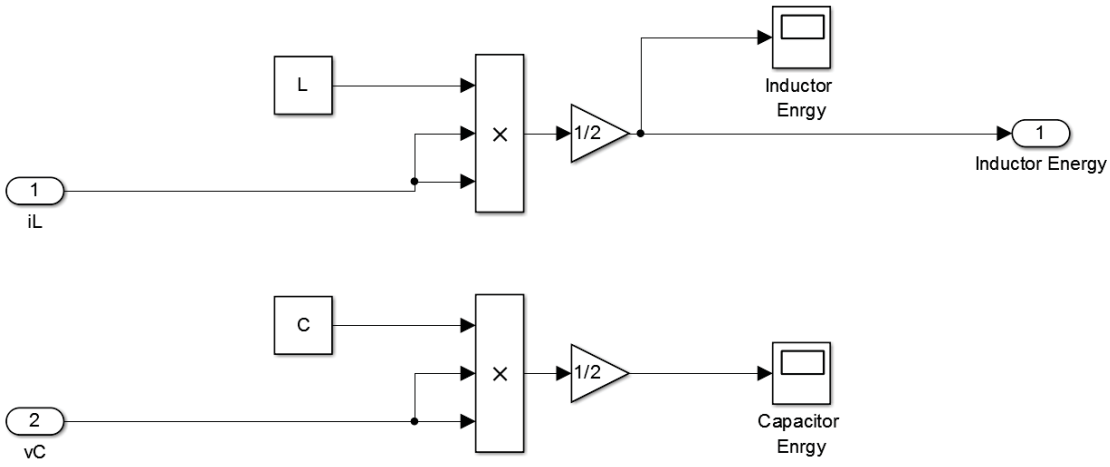

Figure C-3: Energy Calculation Block